frontiers in Microbiology

ORIGINAL RESEARCH
published: 05 November 2020
doi: 10.3389/fmicb.2020.592615

Manganese Depletion Leads to Multisystem Changes in the Transcriptome of the Opportunistic Pathogen *Streptococcus sanguinis*

*Tanya Puccio, Karina S. Kunka, Bin Zhu, Ping Xu and Todd Kitten**

Philips Institute for Oral Health Research, Virginia Commonwealth University, Richmond, VA, United States

Streptococcus sanguinis is a primary colonizer of teeth and is typically considered beneficial due to its antagonistic relationship with the cariogenic pathogen *Streptococcus mutans*. However, *S. sanguinis* can also act as an opportunistic pathogen should it enter the bloodstream and colonize a damaged heart valve, leading to infective endocarditis. Studies have implicated manganese acquisition as an important virulence determinant in streptococcal endocarditis. A knockout mutant lacking the primary manganese import system in *S. sanguinis*, SsaACB, is severely attenuated for virulence in an *in vivo* rabbit model. Manganese is a known cofactor for several important enzymes in *S. sanguinis*, including superoxide dismutase, SodA, and the aerobic ribonucleotide reductase, NrdEF. To determine the effect of manganese depletion on *S. sanguinis*, we performed transcriptomic analysis on a Δ*ssaACB* mutant grown in aerobic fermentor conditions after the addition of the metal chelator EDTA. Despite the broad specificity of EDTA, analysis of cellular metal content revealed a decrease in manganese, but not in other metals, that coincided with a drop in growth rate. Subsequent supplementation with manganese, but not iron, zinc, or magnesium, restored growth in the fermentor post-EDTA. Reduced activity of Mn-dependent SodA and NrdEF likely contributed to the decreased growth rate post-EDTA, but did not appear entirely responsible. With the exception of the Dps-like peroxide resistance gene, *dpr*, manganese depletion did not induce stress response systems. By comparing the transcriptome of Δ*ssaACB* cells pre- and post-EDTA, we determined that manganese deprivation led to altered expression of diverse systems. Manganese depletion also led to an apparent induction of carbon catabolite repression in a glucose-independent manner. The combined results suggest that manganese limitation produces effects in *S. sanguinis* that are diverse and complex, with no single protein or system appearing entirely responsible for the observed growth rate decrease. This study provides further evidence for the importance of this trace element in streptococcal biology. Future studies will focus on determining mechanisms for regulation, as the multitude of changes observed in this study indicate that multiple regulators may respond to manganese levels.

Keywords: *Streptococcus sanguinis*, infective endocarditis, manganese, transcriptome, fermentor, carbon catabolite repression, CcpA

OPEN ACCESS

Edited by:
Catherine Ayn Brissette, University of North Dakota, United States

Reviewed by:
Jessica Kajfasz, University of Florida, United States
JoAnne Stubbe, Massachusetts Institute of Technology, United States

***Correspondence:**
Todd Kitten
tkitten@vcu.edu

Specialty section:
This article was submitted to Microbial Physiology and Metabolism, a section of the journal Frontiers in Microbiology

Received: *07 August 2020*
Accepted: *07 October 2020*
Published: *05 November 2020*

Citation:
Puccio T, Kunka KS, Zhu B, Xu P and Kitten T (2020) Manganese Depletion Leads to Multisystem Changes in the Transcriptome of the Opportunistic Pathogen Streptococcus sanguinis. Front. Microbiol. 11:592615. doi: 10.3389/fmicb.2020.592615

INTRODUCTION

Streptococcus sanguinis is a facultative anaerobe that is typically found in much greater abundance at healthy oral sites than in carious lesions or diseased gingiva (Stingu et al., 2008; Belda-Ferre et al., 2012; Griffen et al., 2012; Gross et al., 2012; Giacaman et al., 2015). The *S. sanguinis* genome encodes a variety of adhesins (Xu et al., 2007; Bensing et al., 2018) that allow it to act as one of the primary colonizers of the salivary pellicle (Socransky et al., 1977; Kolenbrander et al., 2010). It has the capacity to produce (Garcia-Mendoza et al., 1993; Kreth et al., 2008) and survive in (Xu et al., 2014) high concentrations of hydrogen peroxide (H_2O_2), which allows it to compete against the dental caries pathogen *Streptococcus mutans* (Kreth et al., 2005). These traits, which have evolved to ensure survival in the highly diverse oral cavity, also make *S. sanguinis* an opportunistic pathogen (Das et al., 2009; Turner et al., 2009; Bensing et al., 2019). Dental procedures (Kinane et al., 2005; Forner et al., 2006; Lockhart et al., 2008), routine oral hygiene practices (Silver et al., 1977, 1979; Moreillon and Que, 2004), mastication (Sreenivasan et al., 2017), and poor oral hygiene (Kholy et al., 2015) can all damage the oral mucosa, allowing bacteria to enter the bloodstream. *S. sanguinis* and certain other bacterial species can bind to cardiac vegetations composed of platelets and fibrin that form on damaged heart valves and endocardium (Lee et al., 2001), leading to the disease infective endocarditis (IE) (Moreillon et al., 2002; Widmer et al., 2006). Recent studies estimate that IE affects more than 40,000 people each year in the United States and kills 12–40% (Bor et al., 2013; Cahill et al., 2017; Jamil et al., 2019) due to complications such as congestive heart failure and stroke (Bashore et al., 2006). In the United States, prevention depends upon antibiotic prophylaxis prior to dental procedures for at-risk patients (Wilson et al., 2007). The economic burden, potential for side effects, and questionable efficacy (Dayer and Thornhill, 2018; Thornhill et al., 2018; Quan et al., 2020) of this practice, as well as the increasing prevalence of antibiotic resistance (Dodds, 2017) are all pressing concerns.

Manganese (Mn) is an essential human micronutrient and has been linked to virulence in many human pathogens, including streptococci (Kehres and Maguire, 2003; Papp-Wallace and Maguire, 2006; Eijkelkamp et al., 2015). Mn has been shown to play an important role in oxidative stress tolerance through several mechanisms: (i) serving as a cofactor for enzymes that break down reactive oxygen species (ROS), (ii) substituting for iron (Fe) in enzymes when cells experience oxidative stress in order to prevent Fenton reaction-mediated damage, and (iii) reacting with superoxide radicals when complexed with small molecules such as bicarbonate (Waters, 2020).

Previous work from our lab established that the ABC transporter SsaACB is important for Mn transport and essential for virulence in a rabbit model of IE (Crump et al., 2014; Baker et al., 2019; Murgas et al., 2020). In *S. sanguinis*, Mn acts as a cofactor for superoxide dismutase (SodA) (Parker and Blake, 1988; Poyart et al., 1988) and the aerobic class 1b ribonucleotide reductase (NrdEF) (Makhlynets et al., 2014; Rhodes et al., 2014). Loss of SodA activity alone cannot account for the reduction in virulence (Crump et al., 2014). NrdEF activity is essential for virulence (Rhodes et al., 2014), but it is likely that these are not the only two Mn-cofactored enzymes or Mn-dependent pathways in *S. sanguinis*. In a previous microarray analysis of Mn depletion in the closely related species *Streptococcus pneumoniae* (Ogunniyi et al., 2010), it was found that only a few genes were differentially expressed in response to either deletion of the pneumococcal SsaB ortholog PsaA, or growth in media without supplemental Mn. However, these data alone are insufficient to explain the decreased growth of these mutants in low-Mn media. In this study, we sought to determine the overall effect of Mn depletion on the transcriptome of *S. sanguinis* in an attempt to identify other Mn-dependent pathways. Here we report that while there were some similarities with this previous study, we found a larger number of differentially expressed genes, providing new insights into the role of Mn in streptococci.

RESULTS

Selection of Fermentor Growth Conditions for Mn Depletion

For this study, we were interested in measuring transcriptional changes resulting from Mn depletion in metabolically active cells. We also wanted to examine the cells as they transitioned from Mn replete conditions to Mn insufficiency, a task that would most easily have been accomplished by addition of a strong and selective Mn chelator to growing cells. However, we were aware of no such chelator. We therefore explored the use of the non-specific chelator EDTA in conjunction with an Δ*ssaACB* mutant. This mutant was previously found to be deficient in Mn and Fe transport and aerobic growth in low-Mn media (Murgas et al., 2020).

We achieved reproducible, large-scale growth in a fermentor using Brain Heart Infusion (BHI) broth. Typical chemostat conditions (Burne and Chen, 1998) could not be identified that supported growth of the SK36 wild-type (WT) strain but not the Δ*ssaACB* mutant, even when aeration was increased (data not shown). However, we found that when the dilution rate was increased to 0.875 vessel volumes per h, addition of 100 μM EDTA to both the fermentor vessel and media carboy dramatically reduced the optical density ($OD_{840-910}$) of the Δ*ssaACB* mutant cultures (**Supplementary Figure S1A**), while not affecting the WT strain (**Supplementary Figure S1B**). The effect of EDTA addition on the OD of the Δ*ssaACB* cultures typically became apparent after 38 min (**Supplementary Figure S1** inset). The addition of EDTA slowed the growth of Δ*ssaACB* but did not kill the cells entirely because when the media pumps were shut off ∼80 min post-EDTA addition, the OD began to increase immediately (data not shown).

To determine if a lack of available Mn caused the EDTA-dependent reduction in the Δ*ssaACB* growth rate, samples of both WT and Δ*ssaACB* were collected at T_{-20}, T_{10}, T_{25}, and T_{50}, where 100 μM EDTA was added to the vessel at T_0 (**Supplementary Figure S1**). Washed cells were analyzed using inductively coupled plasma optical emission spectroscopy (ICP-OES) (**Figure 1**). EDTA addition to WT did not significantly alter cellular levels of any of the four metals measured—Mn,

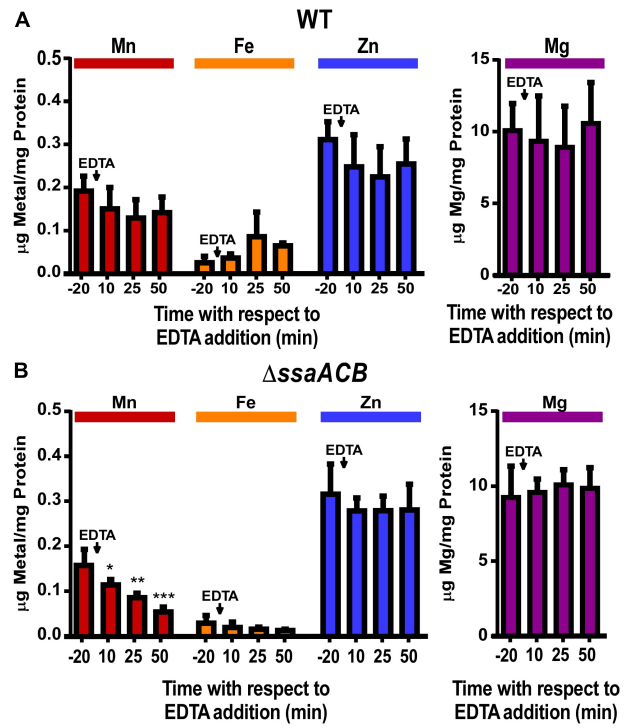

FIGURE 1 | Effect of EDTA on metal content of fermentor-grown WT and Δ*ssaACB* cells. Aerobic fermentor-grown WT **(A)** and Δ*ssaACB* **(B)** cells were collected at each time point and analyzed for cellular metal content using ICP-OES. Means and standard deviations of three replicates are shown. Significance was determined either by repeated measures ANOVA or by one-way ANOVA if matching was not effective, with a Tukey-Kramer multiple comparisons test to T_{-20}. $^{*}P \leq 0.05$, $^{**}P \leq 0.01$, $^{***}P \leq 0.001$. Time points not labeled were not significantly different from T_{-20}. For Fe, two T_{-20} replicates in **(A)** and at least two replicates for each time point in **(B)** were below the limit of detection.

Fe, zinc (Zn), or magnesium (Mg) (**Figure 1A**). Mn was the only metal significantly reduced in the post-EDTA samples as compared to pre-EDTA for Δ*ssaACB* (**Figure 1B**). Fe levels were low in the Δ*ssaACB* mutant (**Figure 1B**), consistent with previous results that this mutant transports less Fe than WT (Murgas et al., 2020). Fe, Zn, and Mg levels were not significantly affected by EDTA addition (**Figure 1**). Cobalt and copper levels were at or below the limit of detection in both strains (data not shown).

As another test of metal specificity, 100 µM of either Mn^{2+} or Fe^{2+} was added to the vessel 70 mins post-EDTA addition. The addition of Mn^{2+} eliminated, and then reversed, the post-EDTA decline in OD, while Fe^{2+} had no discernible effect (**Supplementary Figure S2**). The metal content of samples collected 10 mins after addition of Mn^{2+} or Fe^{2+} (T_{80}) revealed that both Mn and Fe were taken up by cells, resulting in significantly higher levels than at T_{-20} (**Supplementary Figure S3**). Although neither Zn nor Mg levels were significantly affected by addition of EDTA (**Figure 1**), 100 µM of either Zn^{2+} or Mg^{2+} was added at T_{70} for at least two fermentor runs each and, like Fe^{2+}, neither produced any apparent effect (data not shown).

Overview of Transcriptional Response of *S. sanguinis* to Mn Depletion

In order to assess the impact of Mn depletion on the *S. sanguinis* transcriptome, RNA sequencing (RNA-seq) analysis was performed on Δ*ssaACB* fermentor samples collected at the same time points as above (**Supplementary Figure S1A**). Principal component analysis (PCA) revealed that the samples from each time point clustered together, indicating minimal variation between independent replicates (**Figure 2A**). The T_{10} samples overlapped slightly with T_{-20}, indicating few early changes in gene expression. The dissimilarities of the RNA-seq profiles were greater at T_{25} and T_{50}, suggesting that EDTA treatment increasingly affected the gene expression of Δ*ssaACB* during the period tested.

Volcano plot analysis of differentially expressed genes (DEGs; defined as $|\log_2| \geq 1$, adjusted *P*-value ≤ 0.05) comparing post-EDTA time points to the pre-EDTA time point revealed that there were only 48 (2.1%) and 139 (6.1%) DEGs at T_{10} and T_{25}, respectively (**Figure 2B**). In contrast, at 50 mins post-EDTA, 407 genes (17.9%) were differentially expressed, with a number of genes more severely downregulated (**Figure 2B**). Consistent with these results, the growth rate of Δ*ssaACB* decreased dramatically between T_{25} and T_{50} (**Supplementary Figure S1A**).

Gene classification analysis of DEGs at T_{50} using KEGG annotations revealed that genes involved in sugar metabolism were highly enriched, with phosphotransferase systems (PTS), fructose/mannose transport, and pyruvate metabolism all in the top 12 most highly enriched pathways (**Figure 2C**). Other highly enriched pathways included amino acid metabolism, ribosomes, oxidative phosphorylation (ATP synthases), and biosynthesis of coenzymes and various secondary metabolites (**Figure 2C**).

RNA-seq trends for several genes of interest with moderate to high expression level changes were validated by measuring mRNA levels of fermentor samples via quantitative reverse transcriptase polymerase chain reaction (qRT-PCR) (**Supplementary Figure S4**). The relative expression levels observed in the qRT-PCR experiments largely replicated the trends observed in the RNA-seq analysis.

In the following sections, we highlight results we believe to be most important.

Regulation of Metal Transport Genes

As seen in **Figure 1**, Mn was the only tested metal whose cellular concentration was decreased upon addition of EDTA to Δ*ssaACB* cells. To further investigate the impact of EDTA on metal transport, we examined the expression of metal transport genes (**Figure 3**). The kanamycin (Kan) resistance gene *aphA-3* that replaced the Mn transporter operon, *ssaACB*, in this mutant strain was upregulated in all three post-EDTA time points (**Figure 3**). This is consistent with previous results from our lab showing Mn-dependent repression of SsaB expression as measured by western blot (Crump et al., 2014).

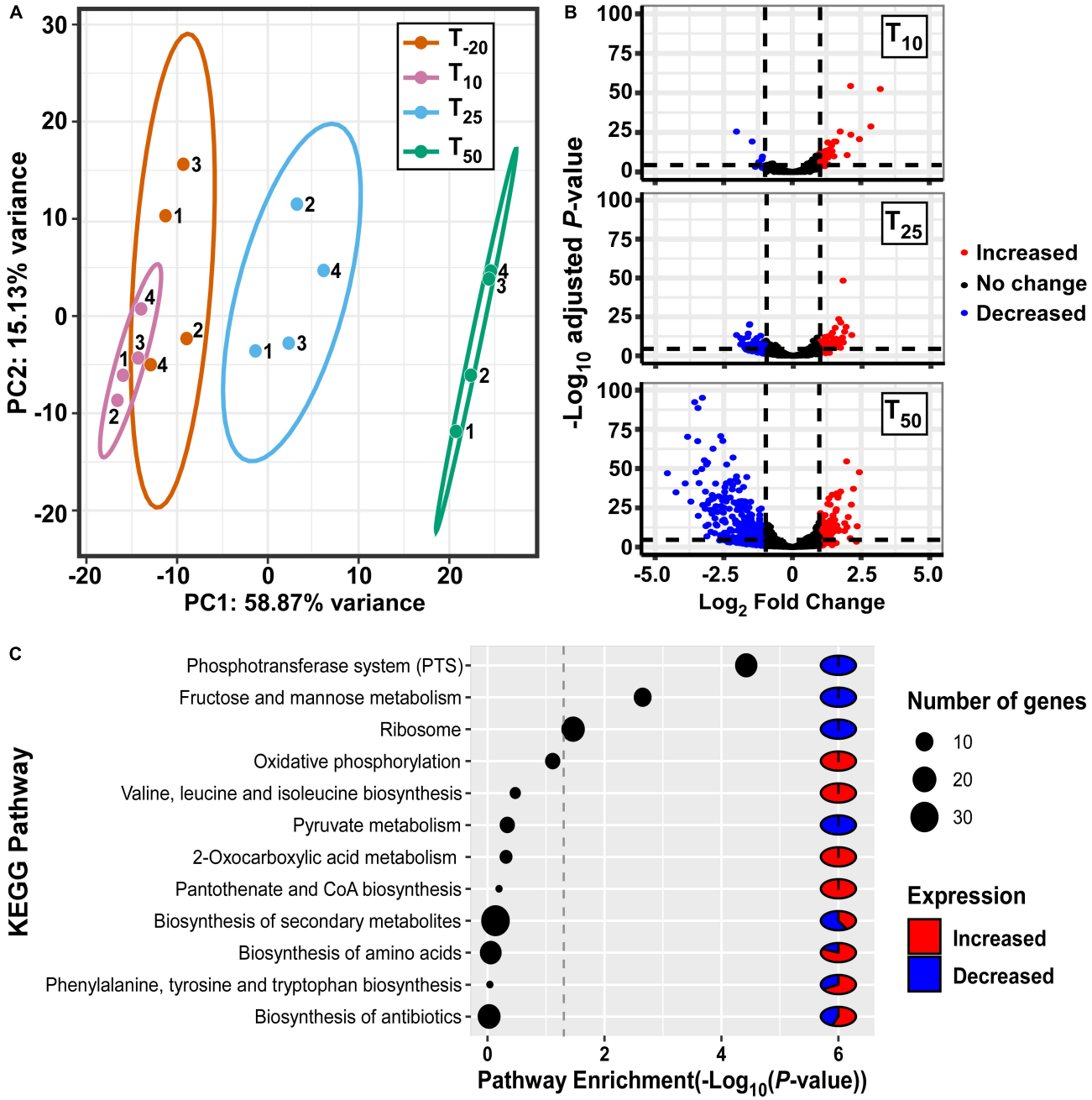

FIGURE 2 | Analysis of gene expression in fermentor-grown *S. sanguinis* Δ*ssaACB* mutant cells. **(A)** Principal component analysis of the RNA-seq samples as determined by the pcaExplorer package for R. Replicates are labeled by fermentor run number. Ellipses are drawn around the 95% confidence interval for each time point. **(B)** Volcano plots comparing each post-EDTA time point to T_{-20} were generated using $\log_2$ fold changes from Geneious in the EnhancedVolcano package for R. Genes that are upregulated in the post-EDTA time point are positive on the x-axis (right) and those that are downregulated are negative (left). Genes exhibiting $|\log_2$ fold change$| > 1$ are depicted by either red (>1) or blue (<1) spheres. **(C)** Pathway enrichment analysis of differentially expressed genes at T_{50} using DAVID classification of genes and KEGG annotations.

Given that the cells were Mn-depleted after EDTA addition (**Figure 1**), it was surprising to see the upregulation at T_{50} of genes encoding putative orthologs of Mn-export proteins MntE (Rosch et al., 2009; Martin and Giedroc, 2016) and MgtA (Martin et al., 2019) of the closely related species *S. pneumoniae* (**Figure 3**). Expression of *mntE* was found to be constitutive (Martin and Giedroc, 2016) and *mgtA* expression was found to be positively regulated by Mn through a metal-dependent riboswitch (Martin et al., 2019). We therefore sought to test whether Δ*mntE* and Δ*mgtA* mutants generated previously in

	Locus Tag	Annotation	TPM	Log_2 Ratio			
			T_{-20}	T_{10}/T_{-20}	T_{25}/T_{-20}	T_{50}/T_{-20}	Log_2 Ratio
Metal Transport Regulators	SSA_0135	*adcR*, MarR family transcriptional repressor	44	-0.79	**0.97**	-0.16	2.5
	SSA_0256	*ssaR*, DxtR family transcriptional repressor	195	-0.19	**-0.50**	0.07	2.0
	SSA_0686	*perR*, Fur family transcriptional repressor	367	-0.11	0.03	**0.39**	1.5
Mn Transport	SSA_0260	*aphA-3* (kanamycin resistance gene replacing *ssaACB)*	563	0.28	**0.75**	**0.96**	1.0
	SSA_0299	VIT family protein	36	0.38	**0.99**	**1.21**	0.5
	SSA_0851	*mntE*, Mn efflux protein	96	0.31	**0.53**	**1.17**	0.0
	SSA_0866	*mgtA*, Mn/Ca exporter	550	0.23	0.28	**0.52**	-0.5
	SSA_1413	GufA-like, ZIP family protein	119	-0.30	-0.33	**-0.92**	-1.0
Fe Transport	SSA_0299	VIT family protein	36	0.38	**0.99**	**1.21**	-1.5
	SSA_0461	*pefC*, heme exporter	144	0.00	-0.08	-0.20	-2.0
	SSA_1129	Periplasmic iron transport lipoprotein	342	0.03	0.01	-0.01	-2.5
	SSA_1130	Iron-dependent peroxidase	117	0.00	0.31	**0.52**	-3.0
	SSA_1131	High-affinity Fe^{2+}/Pb^{2+} permease	150	0.26	**0.43**	**0.73**	-3.5
	SSA_1413	GufA-like, ZIP family protein	119	-0.30	-0.33	**-0.92**	-4.0
	SSA_1578	ABC-type Fe^{3+}-siderophore transport system, permease component	75	0.12	-0.34	-0.34	-4.5
	SSA_1579	ABC-type Fe^{3+}-siderophore transport system, ATPase component	88	-0.10	-0.43	**-0.63**	
	SSA_1581	Hemin ABC transporter	121	0.06	-0.41	-0.45	
	SSA_1741	ABC-type Fe^{3+}-siderophore transport system, ATPase component	92	0.07	-0.23	-0.01	
	SSA_1742	ferrichrome-binding protein	113	0.17	-0.13	0.28	
	SSA_1743	ABC-type Fe^{3+}-siderophore transport system, permease component	60	0.04	-0.20	0.15	
	SSA_1744	iron ABC transporter permease	53	0.21	0.00	0.55	
Zn Transport	SSA_0136	*adcC,* Zn ABC transporter, ATPase	39	-0.11	**1.18**	0.62	
	SSA_0137	*adcB,* Zn ABC transporter, permease	45	0.68	**1.78**	**0.75**	
	SSA_0138	*adcA,* Zn ABC transporter, lipoprotein	62	**0.69**	**1.87**	**0.79**	
	SSA_1339	*phtD,* pneumococcal histidine triad protein D	9	**1.18**	**1.92**	-0.34	
	SSA_1340	*adcAIII,* Zn ABC transporter, orphan lipoprotein	8	0.47	0.89	-1.12	
	SSA_1413	GufA-like, ZIP family protein	119	-0.30	-0.33	**-0.92**	
	SSA_1990	*adcAII,* Zn ABC transporter, orphan lipoprotein	17	**0.98**	**1.49**	-0.17	
	SSA_1991	*phtA,* pneumococcal histidine triad protein A	18	**1.03**	**1.55**	-0.20	
	SSA_2321	*czcD,* Zn/Cd efflux protein	126	-0.37	**-1.83**	**-1.19**	
Mg Transport	SSA_0447	CorA-family protein, magnesium/cobalt transporter	290	-0.28	**-0.51**	**-0.50**	
	SSA_0701	CorA-family protein, magnesium/cobalt transporter	559	-0.38	-0.38	**-0.49**	
	SSA_0888	*mgtE*, Mg/Co/Ni transporter	152	**-0.51**	0.20	**0.51**	
	SSA_1734	Mg/Ni transporter, P-Type ATPase	48	0.33	**0.59**	**0.72**	

FIGURE 3 | Expression of metal transport genes post-Mn depletion. Putative metal transport genes are depicted with their average transcripts per million reads (TPM) at T_{-20} and log_2 fold change values for each post-EDTA time point. TPM values greater than 1,000 are full saturation (green). Positive log_2 fold change values (red) indicate genes upregulated after Mn depletion as compared to T_{-20}, while negative values (blue) indicate downregulated genes. Values in bold indicate significant changes in expression by adjusted *P*-value ($\leq$0.05).

S. sanguinis (Xu et al., 2011) exhibited increased Mn sensitivity relative to WT as expected based on previous findings in *S. pneumoniae* (Rosch et al., 2009; Martin et al., 2019). The Δ*mgtA* mutant grew as expected, with a lower final density than WT in BHI with 2 mM added Mn (data not shown). The Δ*mntE* mutant, however, grew just like WT, which was unlike the findings in *S. pneumoniae* (data not shown). We tested up to 10 mM Mn in BHI and Todd Hewitt broth with 1% yeast extract and could not find a Mn concentration that prevented growth of either the Δ*mntE* mutant or WT (data not shown). Initial metal analysis revealed that the Δ*mntE* mutant accumulated slightly more Mn than WT (data not shown). These results indicate that *S. sanguinis* may primarily use MgtA to export excess Mn, and MntE may function differently in *S. sanguinis* than in *S. pneumoniae*. Future studies will elucidate the function of these putative exporters and their transcriptional regulation in *S. sanguinis*.

As seen in **Figure 1**, cellular Zn levels in Δ*ssaACB* were not significantly altered by EDTA addition, despite the high affinity of this chelator for Zn (Perrin and Dempsey, 1974). Zn level maintenance may be due to the higher levels of Zn than Mn in BHI (1.7 ± 0.02 vs. 0.02 ± 0.003 μg mL^{-1}, respectively) (Murgas et al., 2020) or the regulation of Zn transporter genes. *S. sanguinis* possesses orthologs of the Zn ABC transporter AdcCBA of *S. pneumoniae* (Dintilhac and Claverys, 1997), and all three genes were upregulated post-EDTA (**Figure 3**). Expression of the gene encoding the Zn^{2+} and Cd^{2+} efflux protein, CzcD (Nies, 1992), decreased after EDTA addition (**Figure 3**). Thus, cellular Zn levels appear to have been maintained during EDTA treatment by decreasing export of intracellular Zn and increasing import of any remaining bioavailable Zn through regulation of Zn transporters.

We also examined the regulation of other putative Zn-transport proteins. In *S. pneumoniae*, AdcAII and several

	Locus Tag	Annotation	TPM	Log_2 Ratio		
			T_{-20}	T_{10}/T_{-20}	T_{25}/T_{-20}	T_{50}/T_{-20}
Ribonucleotide Reductases	SSA_0768	*nrdF*, aerobic RNR (Mn-dependent)	695	0.16	-0.35	**-0.66**
	SSA_0769	*nrdK*, aerobic RNR	690	0.20	-0.42	**-0.61**
	SSA_0770	*nrdE*, aerobic RNR	582	0.08	-0.38	**-0.66**
	SSA_0771	*nrdH*, aerobic RNR	3534	-0.09	**-0.55**	**-0.54**
	SSA_1668	*fmnG*, flavodoxin	4	-0.03	-0.07	-0.02
	SSA_1683	*fmnI*, flavodoxin	246	-0.05	-0.16	0.12
	SSA_2226	*nrdG*, anaerobic RNR	14	-0.04	0.58	0.54
	SSA_2227	Acetyltransferase	12	-0.43	0.44	0.83
	SSA_2228	Acetyltransferase	12	-0.41	0.11	0.36
	SSA_2229	Hypothetical protein	38	-0.04	0.22	0.41
	SSA_2230	*nrdD*, anaerobic RNR	67	0.09	0.16	**0.44**
	SSA_2263	*nrdI*, flavodoxin component of aerobic RNR	228	-0.22	0.13	0.31
Competence	SSA_2394	*comC*	5935	0.25	-0.41	**-0.95**
	SSA_2379	*comD*	1397	0.34	-0.16	-0.36
	SSA_2378	*comE*	820	**0.45**	0.16	-0.05
	SSA_0016	*comX*	1517	0.53	**0.74**	0.35
	SSA_0184	*comGA*	315	**0.66**	**1.34**	0.38
	SSA_0185	*comGB*	201	**0.91**	**1.58**	**0.67**
	SSA_0186	*comGC*	114	**0.89**	**1.82**	**1.03**
	SSA_0187	*comGD*	182	0.66	**1.64**	**0.99**
	SSA_0188	*comGE*	177	0.55	**1.63**	**1.13**
	SSA_0189	*comGF*	182	0.61	**1.61**	**1.14**
	SSA_0190	*comGG*	226	0.60	**1.58**	**1.19**
	SSA_0715	*comEA*	196	**1.34**	**1.57**	**0.96**
	SSA_0716	*comEC*	118	**1.12**	**1.79**	**1.22**
	SSA_1497	*comEB*	181	0.05	0.11	0.30
	SSA_1835	*comFC*	124	**1.33**	**1.46**	**1.03**
	SSA_1836	*comFA*	166	**1.43**	**1.42**	**0.87**
Mn-Dependent Enzymes in *S. pneumoniae*	SSA_1204	*pgm*, phosphatase	567	**0.71**	-0.13	**-1.24**
	SSA_1260	*deoB*, pentophosphomutase	218	0.11	**-0.47**	**-2.08**
	SSA_1271	*papP*, nucleotide phosphatase	205	0.17	**0.32**	**0.55**
	SSA_1748	*ppaC*, phosphatase	651	0.28	0.24	0.25
	SSA_1846	*phpP*, phosphatase	577	0.30	0.21	0.26
	SSA_2224	*cspB*, capsular phosphate	242	**-0.50**	**-0.74**	**-1.97**
Rel Proteins	SSA_0250	*relA*, bifunctional (p)ppGpp synthetase/hydrolase	102	**-0.68**	-0.02	0.09
	SSA_1210	*relQ*, (p)ppGpp synthetase	188	**1.30**	**0.60**	**-1.09**
	SSA_1795	*relP*, (p)ppGpp synthetase	115	0.21	0.39	**0.91**
Stress Responses+A31:H58A15:H58C44A37:G58CA1:G58	SSA_0009	Ribosome-associated heat shock protein (S4)	389	-0.41	-0.35	-0.31
	SSA_0156	ATPase with chaperone activity, ATP-binding subunit	4	-0.32	-0.41	**-1.27**
	SSA_0225	*groES*, Heat shock protein	114	-0.34	0.59	0.42
	SSA_0226	*groEL*, Heat shock protein	245	-0.09	0.45	0.17
	SSA_0644	*dpr*, Dps-like peroxide resistance protein	473	**1.00**	**1.81**	**1.97**
	SSA_0669	*clpE*, ATP dependent protease	226	0.08	0.18	0.39
	SSA_0721	*sodA*, Mn-cofactored superoxide dismutase	6597	0.14	**-0.79**	**-1.79**
	SSA_1093	*clpX*, ATP-dependent Clp protease ATP-binding subunit	496	0.09	0.18	0.25
	SSA_1136	*clpA*, ATPases with chaperone activity, ATP-binding subunit	17	**0.87**	**0.90**	**-1.03**
	SSA_1731	*clpP*, ATP-dependent Clp protease, proteolytic subunit	1078	0.26	0.07	**-0.29**
	SSA_1745	*csbD*, General stress response protein	6191	-0.77	-0.96	**-2.55**
	SSA_1979	Alkaline-shock protein	1074	0.00	-0.38	**-0.42**
	SSA_2005	*dnaJ*, Chaperone protein	204	-0.11	-0.01	**-0.80**
	SSA_2007	*dnaK*, Chaperone protein	671	0.66	0.14	**-0.56**
	SSA_2008	*grpE*, Molecular chaperone	359	0.39	-0.09	**-1.08**
	SSA_2009	*hrcA*, Heat shock transcription repressor	707	0.04	**-0.71**	**-1.85**
	SSA_2148	Alkaline shock stress response protein	210	-0.02	0.05	-0.15
	SSA_2190	*hslO*, 33 kDa chaperonin	193	-0.26	-0.27	-0.23
	SSA_2199	*clpC*, ATP-dependent Clp protease, ATP-binding subunit	113	-0.24	0.10	0.11

Log_2 Ratio
2.5
2.0
1.5
1.0
0.5
0.0
-0.5
-1.0
-1.5
-2.0
-2.5
-3.0
-3.5
-4.0
-4.5

FIGURE 4 | Expression of select genes post-Mn depletion. Selected genes of interest are depicted with their average TPM at T_{-20} and log_2 fold change values for each post-EDTA time point. TPM values greater than 1,000 are full saturation (green). Positive log_2 fold change values (red) indicate genes upregulated after Mn depletion as compared to T_{-20}, while negative values (blue) indicate downregulated genes. Values in bold indicate significant changes in expression by adjusted *P*-value ($\leq$0.05).

histidine triad proteins also contribute to Zn transport. AdcAII is an orphan lipoprotein of the AdcCBA system (Bayle et al., 2011; Plumptre et al., 2014) and PhtD is a histidine triad protein encoded adjacent to AdcAII (Bersch et al., 2013; Kallio et al., 2014). *S. sanguinis* has two genes, SSA_1340 and SSA_1990, that encode proteins similar to AdcAII, and each is also adjacent to putative histidine triad protein genes, SSA_1339 or SSA_1991. Because AdcAII is more similar to SSA_1990, we have named this protein AdcAII, whereas we have designated SSA_1340 as AdcAIII. Consistent with a potential role in Zn uptake, all four

of these genes were upregulated at T_{25} (**Figure 3**). The relative contribution of each of these proteins to Zn import remains to be determined, although we hypothesize that the upregulation of these genes contributes to the tight maintenance of Zn levels in cells post-EDTA.

Expression data for additional putative metal transporters may be found in **Figure 3**.

Examination of Known Mn-Cofactored Enzymes

Superoxide Dismutase

S. sanguinis possesses a single superoxide dismutase, SodA (Xu et al., 2007), and it is Mn-cofactored (Crump et al., 2014). Our previous study indicated that reduced SodA activity could account for only a portion of the reduced virulence and aerobic serum growth of the Δ*ssaB* mutant (Crump et al., 2014). Expression of *sodA* decreased significantly at both T_{25} and T_{50} despite constant air input (**Figure 4**), which may be due to Mn-dependent positive regulation of transcription (Jakubovics et al., 2002; Eijkelkamp et al., 2014). Given that the fermentor growth conditions do not exactly replicate our previous *in vitro* or *in vivo* assays, we wondered whether SodA would be important here. To answer this question, we grew our Δ*sodA* knockout mutant in the fermentor under the same conditions without EDTA. The Δ*sodA* mutant grew similarly to WT (**Supplementary Figure S5**), indicating that Mn-dependent SodA activity is not essential for aerobic growth under these conditions. While this does not rule out the possibility that reduced SodA activity post-Mn depletion contributed to the reduced growth rate of Δ*ssaACB*, it established that it was not the sole cause, thus encouraging us to investigate other possibilities.

Class Ib Aerobic Ribonucleotide Reductase

The other known Mn-cofactored enzyme in *S. sanguinis* is the aerobic class Ib ribonucleotide reductase (RNR), NrdEF (Makhlynets et al., 2014; Rhodes et al., 2014). RNR enzymes catalyze the production of deoxynucleotides from the corresponding ribonucleotides. It was previously found that mutant strains lacking this enzyme were unable to grow in aerobic conditions, whether in serum or BHI. These studies also suggested that Fe could not substitute for Mn as an RNR cofactor *in vivo*, despite its ability to do so *in vitro*. In addition to a likely decrease in activity, expression of *nrdHEKF* was downregulated after Mn depletion (**Figure 4**). We recently analyzed the metabolome of *S. sanguinis* cells under the same conditions as this study (Puccio et al., 2020). Levels of detected deoxynucleosides and deoxynucleotides in cells increased or remained constant after Mn depletion. Thus, while NrdEF requires Mn for activity, our data suggest that deoxynucleotides may not be a limiting factor for growth in our study.

Mn-Dependent Phosphatases

In the related species *S. pneumoniae*, there are six additional enzymes (**Figure 4**) that have been found to have Mn cofactors (Kuipers et al., 2016; Martin et al., 2017). Orthologs of all six enzymes are encoded in the *S. sanguinis* genome. Although each is a reciprocal best hit with its *S. pneumoniae* counterpart by NCBI BlastP, their functions have not been confirmed. Pgm and CspB are phosphatases that have been implicated in capsule biosynthesis in *S. pneumoniae,* although *S. sanguinis* lacks a true capsule. DeoB is a phosphopentomutase that connects the pentose phosphate pathway to purine biosynthesis and was also significantly downregulated at T_{50}. Expression of *papP*, encoding a nucleotide phosphatase, was significantly increased at the later time points and has been shown to affect membrane lipid homeostasis (Kuipers et al., 2016). A significant morphological difference was observed in Δ*papP* mutants in *S. pneumoniae,* but Δ*ssaACB* cells from the T_{50} sample did not appear morphologically different from cells at T_{-20} (data not shown). Of note, we observed changes in fatty acid synthesis under these same fermentor growth conditions (Puccio et al., 2020), suggesting that activity of PapP may be reduced but not to the extent that it substantially affects morphology.

Genes encoding the other two phosphatases, PhpP and PpaC, were not differentially expressed at any time point (**Figure 4**). While this indicates the lack of a Mn-dependent regulation mechanism, it does not rule out the possibility that their activity was decreased due to reduction of Mn. PhpP is a serine/threonine protein phosphatase that is a key regulator of cell division and has been shown to be regulated by the bioavailable Zn:Mn ratio in *S. pneumoniae* (Martin et al., 2017). While the Zn:Mn ratio did increase over time in our study (**Table 1**), morphology did not differ from T_{-20} (data not shown), indicating that PhpP may not be affected by Mn limitation under these conditions. In our recent study, loss of PhpP did not significantly affect the growth of *S. sanguinis* in serum, a Mn-limited medium (Zhu et al., in press), which indicates that it is likely not responsible for the growth rate decrease observed here. The last phosphatase, PpaC, is essential for *S. sanguinis* (Xu et al., 2011), so if PpaC activity was decreased due to Mn depletion, this could have contributed to the decreased growth rate phenotype observed post-EDTA. Further studies utilizing the knockout mutants of each non-essential phosphatase (Xu et al., 2011) or an approach such as CRISPR interference (Shields et al., 2020) for PpaC would enhance our understanding of the relative contributions of each phosphatase to the growth and morphology of *S. sanguinis*.

(p)ppGpp Hydrolase Domain

In streptococci and enterococci, Mn acts as a cofactor for the hydrolase domain of the bifunctional (p)ppGpp synthetase/hydrolase, RelA (also called RSH for RelA/SpoT Homologs) (Mechold et al., 1996). As an alarmone, (p)ppGpp serves as an effector of the stringent response in bacteria

TABLE 1 | Zn:Mn ratios in fermentor grown cells.

Strain	T_{-20}	T_{10}	T_{25}	T_{50}
WT	1.64	1.66	1.75	1.81
Δ*ssaACB*	2.02	2.47*	3.30*	5.36*

*Values indicate ratios of Zn concentrations as compared to those of Mn. Concentrations were determined by ICP-OES and significance was determined by one-way ANOVA with a Tukey-Kramer multiple comparisons test vs. T_{-20} where * indicates $P \leq 0.05$.*

(Irving and Corrigan, 2018). Expression of *relA* was unchanged after EDTA addition, and expression of the other two small alarmone synthetase genes, *relP* and *relQ* (Lemos et al., 2007), were significantly increased and decreased, respectively (**Figure 4**). Both RelP and RelQ were found to produce less (p)ppGpp than RelA in *S. mutans* (Lemos et al., 2007) and appear to be important during different environmental conditions or growth stages in gram-positive bacteria (Yang et al., 2019).

In an attempt to determine whether loss of hydrolase activity in RelA could account for the phenotypes we observed in Mn-depleted cells, we attempted to construct a hydrolase-deficient mutant by altering specific residues (R44, H62, T151) shown by Hogg et al. (2004) to be important for (p)ppGpp hydrolase, but not synthetase activity. Similar to Kaspar et al. (2016), we were unable to generate any of the three point mutants without unintended mutations arising in other regions of the gene (data not shown). This indicates that hydrolase activity may be essential for growth of *S. sanguinis*. We then obtained strains from the comprehensive *S. sanguinis* mutant knockout library created by Xu et al. (2011) that were deleted for each of the *rel* genes. We also generated a rel^0 strain by knocking out all three *rel* genes utilizing a markerless mutagenesis system (Xie et al., 2011; Cheng et al., 2018). We also made these *rel* knockout mutants in the Δ*ssaACB* background. We then assessed the growth of these mutants in aerobic serum-our *in vitro* model for infective endocarditis (Crump et al., 2014). As shown in **Figure 5**, neither Δ*relP* nor Δ*relQ* grew to a density that differed significantly from its parent strain, whether in the WT or Δ*ssaACB* background. Likewise, in both backgrounds Δ*relA* was more severely attenuated than rel^0, suggesting that is it more detrimental to lose activity of RelA than to lack all (p)ppGpp.

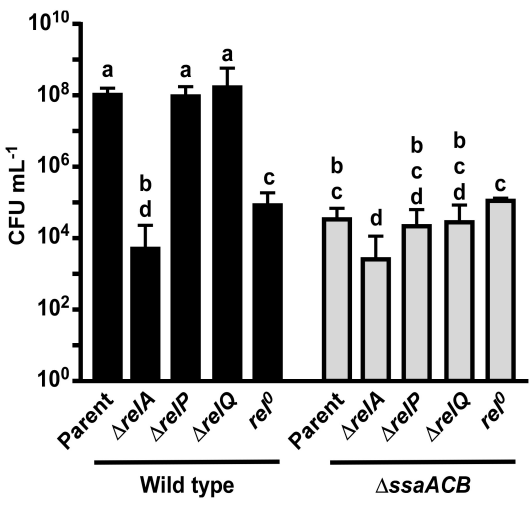

FIGURE 5 | Aerobic serum growth of *rel* mutants. Various *rel* mutants were grown for 24 h in 6% O_2 in pooled rabbit serum. The means and standard deviations of at least three replicates are displayed. Significance was determined by one-way ANOVA with a Tukey-Kramer multiple comparisons test. T_{24} bars with the same letter are not significantly different from each other. Initial culture concentrations were measured (not shown) and found to be not significantly different by one-way ANOVA.

Assessment of Stress and Stress Responses in Mn-Depleted Cells Through Gene Expression

We next sought to determine whether the RNA-seq data suggested anything concerning stresses experienced by the cells. Expression of various stress response genes were assessed, and most were either downregulated or unchanged at T_{50} (**Figure 4**), indicating that the reduced growth rate is likely not due to an overwhelming stress response. The only stress response-related gene to show a significant increase in expression at T_{50} was that encoding the Dps-like peroxide resistance protein, Dpr (Yamamoto et al., 2000). Dpr is a ferritin-like protein that has been shown to be imperative for oxidative stress tolerance in several streptococci (Yamamoto et al., 2000, 2002; Pulliainen et al., 2003; Brenot et al., 2005), including *S. sanguinis* SK36 (Xu et al., 2014).

S. sanguinis is known to generate copious amounts of H_2O_2, presumably to more effectively compete against other oral species, such as the caries-forming pathogen *S. mutans* (Kreth et al., 2005; Chen et al., 2011). Simple Mn compounds have been reported to prevent oxidative stress by catalyzing the decomposition of H_2O_2 (Liochev and Fridovich, 2004) and superoxide (Barnese et al., 2008, 2012). We observed a significant decrease in expression of the gene encoding the H_2O_2-generating enzyme pyruvate oxidase, *spxB* (Spellerberg et al., 1996; Chen et al., 2011), at T_{25} and T_{50} (**Figure 6A**). To determine whether the decreased growth rate of the Δ*ssaACB* strain during aerobic fermentor growth after Mn depletion was due to excess H_2O_2 generation or the inability of cells to cope with H_2O_2 without Mn, H_2O_2 levels were measured in spent supernatant. Concentrations ranged between 1 and 5 μM (**Figure 6B**), far lower than has been observed in previous studies employing SK36 (Kreth et al., 2008) despite the constant influx of air into the vessel. H_2O_2 levels also decreased significantly at T_{25} and T_{50} as compared to T_{-20} (**Figure 6B**), which correlates with the decreased expression of *spxB* (**Figure 6A**). These results indicate that oxidative stress related to excess H_2O_2 levels is unlikely to be the cause of the growth rate decrease observed upon Mn depletion.

Analysis of Carbon Catabolite Repression and Sugar Transport

Examination of DEG clusters revealed that the majority of those thought to transport sugars were downregulated (**Supplementary Table S2**), and of these, the majority belonged to the PTS family, which is regulated by carbon catabolite repression (CCR). CCR is a regulatory mechanism that gives bacteria the ability to utilize carbon sources in order of preference (Gorke and Stulke, 2008). In gram-positive bacteria, a carbon catabolite protein such as CcpA binds to catabolite responsive elements (*cre*) and represses transcription of genes encoding non-preferred carbon source transport and utilization systems (Warner and Lolkema, 2003). To determine the extent to which CcpA binding could be responsible for the observed downregulation, *cre* sites identified previously by RegPrecise (Novichkov et al., 2013) and by our custom searches were collected and compared. Using these methods, 393 putative binding sites were identified

A

		TPM	Log_2 Ratio		
		T_{-20}	T_{10}/T_{-20}	T_{25}/T_{-20}	T_{50}/T_{-20}
SSA_0391	*spxB*, pyruvate oxidase	1824	0.21	**-0.87**	**-2.46**

B

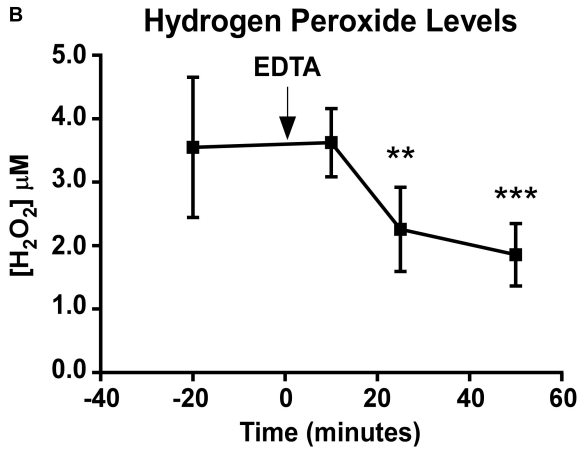

FIGURE 6 | Quantitation of *spxB* expression and hydrogen peroxide in Δ*ssaACB* fermentor cultures. **(A)** Expression of the *spxB* gene in fermentor-grown Δ*ssaACB* cells as determined by RNA-seq analysis. Average TPM at T_{-20} and log_2 fold change values for each after Mn depletion time point are displayed. TPM values greater than 1,000 are full saturation (green). Positive log_2 fold change values (red) are genes upregulated in after Mn depletion samples as compared to T_{-20}, while negative values (blue) indicate downregulated genes. Values in bold indicate significant changes in expression by adjusted *P*-value (≤0.05). **(B)** H_2O_2 levels of the BHI culture supernatant were measured at each time point. Means and standard deviations of at least four replicates are shown. Significance was determined by one-way ANOVA with a Tukey-Kramer multiple comparisons test, comparing each post-EDTA time point to T_{-20}. $^{**}P \leq 0.01$, $^{***}P \leq 0.001$.

(**Supplementary Table S2**). Several PTS and sugar ABC transport genes were predicted to have 5' *cre* sites, the majority of which were downregulated at T_{50}. Other genes known to be CcpA-regulated in SK36, such as *spxB* (Zheng et al., 2011; Redanz et al., 2018), were downregulated as well. This is surprising given that the glucose-containing media was replenished at a constant and rapid rate throughout the experiment, indicating that there could be a Mn-related mechanism for CcpA repression. Cells also did not appear to be starved for glucose; when excess glucose (1.8%) was added to the media, the post-EDTA growth rate was similar to that of normal BHI, which contains 0.2% glucose (data not shown). This is not entirely unexpected, as it has been established by Redanz et al. (2018) that CcpA repression of *spxB* in *S. sanguinis* is glucose-independent.

Several CcpA-regulated genes were annotated as amino acid transporters and synthetases, which led us to examine the expression of genes with these putative functions. Many of these genes were differentially expressed (**Supplementary Figure S6**), which may be due to the intertwined nature of amino acid and carbohydrate metabolism (Radin et al., 2016). We also observed decreased expression of large, contiguous loci encoding ethanolamine utilization (Fox et al., 2009; Kaval and Garsin, 2018; Kaval et al., 2019), a type IV pilus system (Chen et al., 2019), and CRISPR-associated proteins (Makarova et al., 2015; Gong et al., 2020; **Supplementary Figure S7**), which are all also tied to CcpA-regulation (Bai et al., 2019).

DISCUSSION

Only two enzymes have been confirmed to be Mn-dependent in *S. sanguinis*, and few others have been identified in other streptococci. Despite this, we observed changes in a wide variety of systems after Mn depletion of the Δ*ssaACB* mutant using EDTA. One possible explanation for this discrepancy is that Mn binds with low affinity to most proteins, resulting in Mn loss or replacement during purification. In fact, initial studies of the aerobic class Ib RNR identified Fe as the exclusive cofactor based on RNR activity *in vitro* and the fact that Fe was present in many different bacterial RNRs heterologously expressed in *E. coli*. Only later was it discovered that these enzymes were Mn-cofactored when natively expressed (Cotruvo and Stubbe, 2012), and despite the *in vitro* activity of both forms of the *S. sanguinis* RNR, only the Mn-cofactored version was active *in vivo* (Makhlynets et al., 2014; Rhodes et al., 2014). Additional Mn-dependent enzymes may have similarly escaped detection. Another possible explanation is that Mn depletion impacts several key regulatory systems, such as CCR and (p)ppGpp, which leads to changes in the expression of many different genes. Mn levels have been found to be related to each of these systems in other gram-positive bacteria (Kehres and Maguire, 2003; Colomer-Winter et al., 2017). Mn depletion does not appear to induce a traditional stress response, although expression of an oxidative stress tolerance protein, Dpr, significantly increased, which is consistent with a recent study on Mn depletion in *S. mutans* (Kajfasz et al., 2020). Here we highlight Mn-related systems we identified in this study of *S. sanguinis* for future investigation.

Mn Depletion Leads to Glucose-Independent Changes in the Regulon of CcpA

Given that BHI contains glucose, it was expected that *S. sanguinis* would preferentially transport and utilize it as a preferred carbon source under standard fermentor conditions. This is supported by the fact that glucose levels decreased in the media after cell growth (Puccio et al., 2020) as well as by the high expression of putative glucose transporters SSA_1752, SSA_1918-1920, and SSA_1298-1300 (Ajdic and Pham, 2007) at T_{-20} (**Supplementary Table S2**). Surprisingly, expression of nearly all sugar transport systems decreased after Mn depletion (**Supplementary Table S2**), despite constant levels of glucose in the cells (Puccio et al., 2020). CcpA is known to repress its own expression in a glucose-dependent manner (Bai et al., 2019), and yet much like the glucose transporters, *ccpA* expression was high at T_{-20} and significantly decreased by T_{50} (**Supplementary Table S2**). Potential explanations could include: (i) 2 g/L glucose in BHI is not sufficient to induce CcpA repression; (ii) other regulatory mechanisms are preventing proper CCR under these conditions; or (iii) much like *spxB*, many other systems in *S. sanguinis* are subject to glucose-independent CcpA repression. Redanz et al. (2018) used 0.3% as the low-glucose condition in their study of

CcpA repression of *spxB* in *S. sanguinis*, whereas Bai et al. (2019) used BHI alone (0.2% glucose) to observe differences in the transcriptome between the WT and Δ*ccpA S. sanguinis* strains. Thus, the glucose concentration in BHI may indeed be low, yet sufficient to induce some repression of its regulon.

It is interesting that Mn depletion leads to an apparent increase in CcpA repression because we are not aware of this having ever been reported. The strongest evidence for CcpA-dependent regulation is *spxB*. In *S. sanguinis*, *spxB* expression has been shown to be positively regulated by SpxA1 (Chen et al., 2012) and VicK (Moraes et al., 2014) and negatively regulated by CcpA (Zheng et al., 2011). The *spxA1* gene was in the top 10% of all genes based on expression at T_{-20} and remained unchanged after EDTA addition (**Supplementary Table S1**), indicating that repression by CcpA is likely responsible for the decrease in *spxB* expression as opposed to changes in induction by SpxA1. The mechanism by which CcpA represses *spxB* expression in *S. sanguinis* is unique from other streptococci in that it is independent of glucose (Redanz et al., 2018). It was previously determined that Mn may play a role in *spxB* expression in *S. pneumoniae*, as a Δ*mntE* mutant in *S. pneumoniae* accumulated Mn and produced more H_2O_2 than WT under excess Mn conditions (Rosch et al., 2009).

The connection between Mn and sugar catabolism is not unprecedented, as previous studies have implicated Mn as important for the activity of carbon catabolism enzymes in other bacteria (Kehres and Maguire, 2003). Additionally, recent studies in *S. pneumoniae* and *S. mutans* have shown that fluctuations in metal homeostasis influence the regulation of carbohydrate metabolism (Burcham et al., 2020; Kajfasz et al., 2020). One possible explanation for the Mn-dependent, glucose-independent CcpA repression observed in our study is the accumulation of the glycolytic intermediate, fructose-1,6-bisphosphate (FBP) during Mn depletion (**Figure 7**). In Firmicutes, phosphorylation of histidine phosphocarrier protein (HPr) to HPr(Ser-P) occurs when FBP and ATP levels are high (Gorke and Stulke, 2008). HPr(Ser-P) then binds to CcpA, which in turn induces the binding of the repressor to *cre* sites on the DNA. Additionally, FBP enhances the binding interaction of HPr(Ser-P) and CcpA, increasing repression. In our concurrent metabolomics study, we found that Δ*ssaACB* cells accumulated FBP at T_{50} after Mn depletion (Puccio et al., 2020), which may explain the strong evidence for CcpA repression. As expected if CcpA were responsible for the changes in expression, we found that 48 out of the 169 DEGs found by Bai et al. (2019) when comparing a Δ*ccpA* mutant to the SK36 WT were changed in the opposite

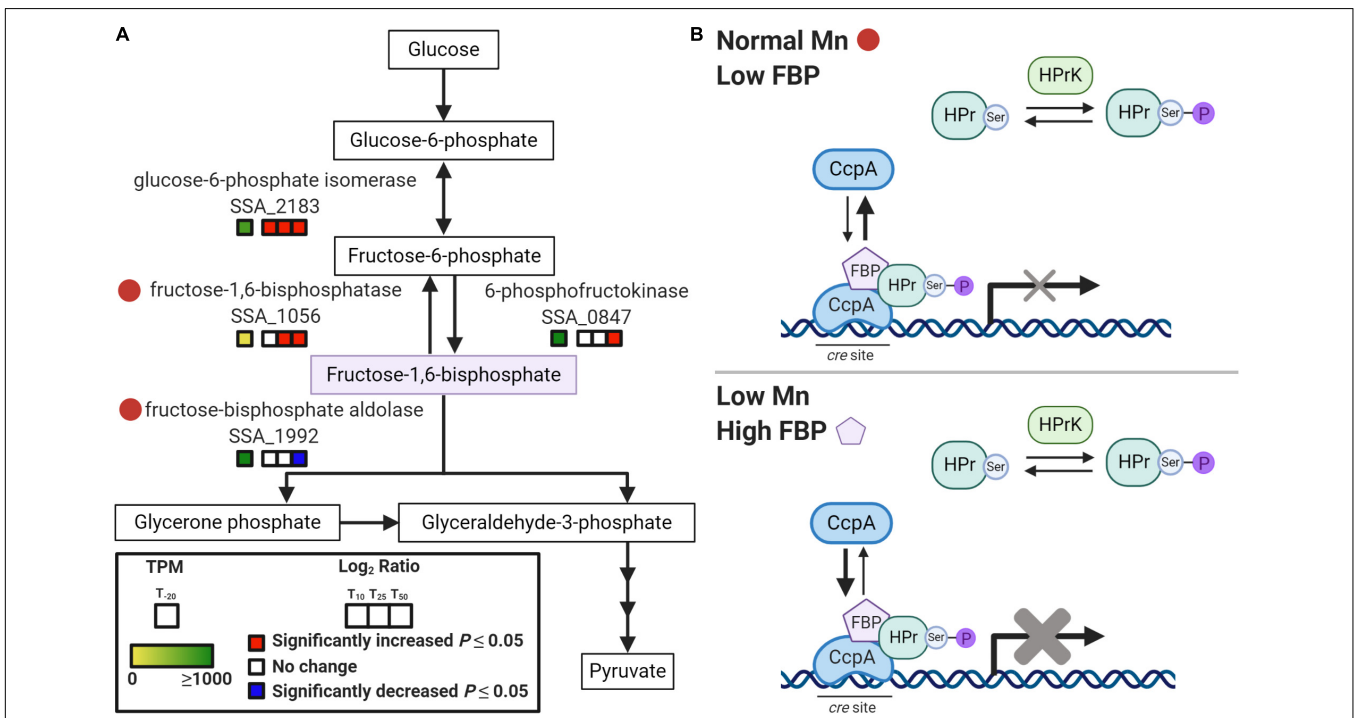

FIGURE 7 | Model of Mn-dependent CcpA repression. **(A)** Depiction of a segment of the glycolysis and gluconeogenesis pathway in *S. sanguinis* from KEGG (Kanehisa and Goto, 2000). Red circles indicate potentially Mn-cofactored enzymes. Gene expression for each post-EDTA time point compared to T_{-20} is indicated by the colored boxes. Significant changes ($P < 0.05$) are indicated by red (increased) or blue (decreased). TPM values at T_{-20} are colored as indicated, with values ≥ 1,000 fully saturated (green). **(B)** Model of Mn-dependent CcpA repression based on CCR in Firmicutes as described by Gorke and Stulke (2008). In the top panel, normal Mn levels in BHI result in low FBP, which leads to less phosphorylation of HPr to HPr(Ser-P) by HPr kinase/phosphorylase (HPrK). With low FBP and HPr(Ser-P), CcpA exists mainly in its free state, unbound to *cre* sites in the DNA. This results in little to no repression of the CcpA regulon. The bottom panel depicts Mn depletion, where reduced activity of fructose-1,6-bisphosphatase and fructose-bisphosphate aldolase leads to an accumulation of FBP. This induces the phosphorylation of HPr so that it is primarily in the HPr(Ser-P) state. Increased FBP levels also enhance binding of CcpA to HPr(Ser-P) and to DNA. This results in augmented repression of the CcpA regulon.

direction as our T_{50} sample. However, 15 significant DEGs were in the same direction, and the remainder were unchanged in our study. Additionally, most of the DEGs we observed in our study did not overlap with those of Bai et al. (2019). This comparison indicates that CcpA-dependent repression could be responsible for some of the changes in expression after Mn depletion, but it does not explain all of the observed results.

To determine potential causes for the accumulation, we examined the enzymes required for synthesizing and catabolizing FBP (**Figure 7A**). Both enzymes responsible for metabolizing FBP, fructose-1,6-bisphosphatase (Fbp; SSA_1056) and fructose-bisphosphate aldolase (Fba; SSA_1992), may require a Mn cofactor according to BRENDA (RRID:SCR_002997)[1] (Jeske et al., 2019). Thus, it is possible that Mn depletion led to reduced activity of both Fba and Fbp and this resulted in accumulation of FBP (Puccio et al., 2020), which in turn induced CcpA repression after Mn depletion (**Figure 7B**). Enzymatic activity assays will be required to determine the true cofactor for these enzymes in *S. sanguinis*, but accumulation of FBP is strong evidence that the activity of at least one enzyme in this pathway is affected by Mn depletion.

Reduced (p)ppGpp Hydrolase Activity May Contribute to the Post-Mn Depletion Phenotype

The relationship between (p)ppGpp and carbon source utilization has been previously established; *S. mutans* strains lacking RelA or all Rel proteins showed delayed growth rates when transitioned from media containing glucose to lactose (Zeng et al., 2018). When we examined the genome for *cre* sites, *relQ* was predicted to have a 5' *cre* site and was downregulated at T_{50} (**Supplementary Table S2**), indicating that it could be under CcpA control. Little is known about the transcriptional regulation of *relA* in streptococci (Nascimento et al., 2008; Irving and Corrigan, 2018), although regulation of activity has been established in other species (Gratani et al., 2018). In *S. mutans*, expression of *relP* is activated by a two-component system, RelRS, which is thought to sense oxidative stressors (Seaton et al., 2011). It was hypothesized by Kim et al. (2012) that (p)ppGpp production by RelP in *S. mutans* may be an attempt by the cell to slow growth to minimize damage from oxygen radicals produced during metabolism. While it was observed in this study that H_2O_2 levels decreased in response to Mn depletion, it is possible that other ROS were present due to a decrease in SodA activity. Thus, increased expression and activity of RelP, in addition to lack of hydrolase activity by RelA, could be at least partly responsible for the reduced growth rate.

In analyzing previous transcriptome studies using Δ*relA* or *rel*^{0} mutants in the related species *S. mutans, S. pneumoniae*, and *Enterococcus faecalis* (Nascimento et al., 2008; Kazmierczak et al., 2009; Colomer-Winter et al., 2019), we noted many expression patterns similar to our study. While these studies utilized different species and growth conditions and thus are not a direct comparison, it is remarkable that reduction in (p)ppGpp levels would lead to similar changes in gene expression as Mn depletion. Of interest to us, several PTS genes were downregulated in all three previous studies. Similar to the results we observed in this study, the *S. pneumoniae* Δ*relA* mutant showed decreased expression of *spxB* and *sodA* (Kazmierczak et al., 2009). These comparisons indicate either that dysregulation of (p)ppGpp levels leads to changes in expression of these genes in response to stress or that decreased activity of the Rel hydrolase domain due to Mn depletion is not responsible for the observed changes in expression of these genes in *S. sanguinis*.

Based on these results, we hypothesize that reduced activity of the RelA hydrolase domain may contribute to the observed reduction in growth rate in the fermentor studies but is not entirely responsible. Specifically, our inability to eliminate the cell's only known (p)ppGpp hydrolase, combined with our finding that the Δ*relA* strains, which also have no hydrolase, exhibited worse growth than *rel*^{0} mutants having no synthetase and therefore no (p)ppGpp, suggests that (p)ppGpp accumulation is highly detrimental to growth. A definitive test of this hypothesis will require measurement of (p)ppGpp levels in fermentor-grown cells. We are currently assessing various approaches for feasibility. In addition, the significant decrease in growth of the Δ*ssaACB* Δ*relA* strain as compared to the Δ*ssaACB* parent shows that there is an additive effect, indicating that the impact of the loss of RelA is not entirely Mn-dependent.

TABLE 2 | Strains used in this study.

Strain	Description	Source or reference
SK36	Human oral plaque isolate	M. Killian, Aarhaus University; Xu et al., 2007
JFP132	Δ*sodA*::*aphA-3*	Crump et al., 2014
JFP169†	Δ*ssaACB*::*aphA-3*	Baker et al., 2019
JFP173‡	Δ*ssaACB*::*tetM*	Baker et al., 2019
SSX_0250	Δ*relA*::*aphA-3*	Xu et al., 2011
JFP259	Δ*relA*::*aphA-3*	This study
JFP260	Δ*ssaACB*::*tetM* Δ*relA*::*aphA-3*	This study
SSX_1210	Δ*relQ*::*aphA-3*	Xu et al., 2011
JFP279	Δ*relQ*::*aphA-3*	This study
JFP281	Δ*ssaACB*::*tetM* Δ*relQ*::*aphA-3*	This study
SSX_1795	Δ*relP*::*aphA-3*	Xu et al., 2011
JFP275	Δ*relP*::*aphA-3*	This study
JFP277	Δ*ssaACB*::*tetM* Δ*relP*::*aphA-3*	This study
JFP276	Δ*relA*::*aphA-3*Δ*relP*	This study
JFP278	Δ*ssaACB*::*tetM* Δ*relA*::*aphA-3*Δ*relP*	This study
JFP280	Δ*relA*::*aphA-3*Δ*relP*Δ*relQ* (*rel*^{0})	This study
JFP282	Δ*ssaACB*::*tetM* Δ*relA*::*aphA-3*Δ*relP*Δ*relQ* (*rel*^{0})	This study
SK36 IFDC	*pheS* ermAM*	Cheng et al., 2018

†*Designated* Δ*ssaACB throughout the manuscript.* ‡*Only used for* Δ*ssaACB strains in* ***Figure 5***.

CONCLUSION

The effect of Mn depletion on a multitude of diverse systems indicates that the impact of Mn is not relegated to only a few

[1]brenda-enzymes.org

enzymes. Depletion of Mn does not induce a traditional stress response, instead inducing what appears to be dysregulation of many different genes that leads to rapid reduction in the growth rate, despite plentiful nutrients and other metals. While decreased function of the known Mn-cofactored enzymes, such as NrdF, SodA, and the hydrolase domain of RelA, likely contributed to the decreased growth rate we observed upon Mn depletion, it is probably a combination of multiple systems leading to the observed phenotype. Additionally, many of the affected systems appear to be regulated by CCR through CcpA-dependent repression in a glucose-independent manner. Future research will focus on determining the respective contribution of each putative Mn-dependent enzyme as well as whether there is a direct relationship between Mn and CCR.

MATERIALS AND METHODS

Bacterial Strains and Growth Conditions

The *S. sanguinis* strain SK36 is a human oral isolate from Mogens Killian, Aarhus University, Denmark. All mutant strains were generated in the SK36 background (**Table 2**) using the primers listed in **Supplementary Table S3**. The Δ*ssaACB* strains were generated previously (Baker et al., 2019) with all three genes replaced with either a kanamycin (Kan) resistance gene, *aphA-3,* or tetracycline (Tet) resistance gene, *tetM*, using gene splicing by overlap extension (SOEing) PCR (Ho et al., 1989). The Δ*ssaACB*::*aphA-3* mutation is non-polar, as confirmed by complementation (Murgas et al., 2020). With the exception of **Figure 5**, all Δ*ssaACB* experiments were completed with the Kan^R strain, JFP169. The Δ*relA*, Δ*relP,* and Δ*relQ* mutants were re-created for this study by amplifying the *aphA-3* gene and flanking DNA from the corresponding, previously created mutants (Xu et al., 2011) using primers from the same study. All PCR products were purified using a Qiagen MinElute PCR kit prior to transformation. Transformations employing antibiotic selection were performed using the protocol described previously (Paik et al., 2005). Briefly, an overnight culture of the parent strain was grown in BD Bacto^{TM} Todd Hewitt broth with horse serum (Invitrogen), then diluted 200-fold and incubated at 37°C. Optical density (OD_{600}) of tube cultures was determined using a Thermo Scientific BioMate 3S UV-VIS spectrophotometer. Knockout construct DNA (100 ng) and *S. sanguinis* competence stimulating peptide (70 ng) were added to the culture (OD_{600} ∼0.07) and incubated at 37°C for 1.5 h prior to selective plating on BHI (BD) agar plates with antibiotics. Kan (Sigma-Aldrich) was added to a final concentration of 500 μg mL^{-1}. All plates were incubated for 24 h at 37°C under anaerobic conditions, where atmospheric composition was adjusted using a programmable Anoxomat Mark II jar-filling system (AIG, Inc.) and a palladium catalyst was included in the jars. All mutants were confirmed to have the expected composition by sequence analysis of the DNA flanking the insertion sites.

To generate the *rel*^{0} strain, Δ*relP* and Δ*relQ* mutations were made using a markerless mutation system described previously (Xie et al., 2011; Cheng et al., 2018). Briefly, the IFDC2 cassette was amplified from the *S. sanguinis* IFDC2 strain and combined with flanking region from *relP* using gene SOEing. The two parent Δ*relA* strains (WT and Δ*ssaACB*::*tetM* backgrounds) were then transformed as described above, plating on BHI agar plates containing 10 μg mL^{-1} erythromycin (Erm; Fisher Scientific). A gene SOEing product merging the two flanking regions of *relP* was then generated. This SOEing product was then used to transform the Erm^R colonies from the first transformation. Immediately prior to plating on agar plates containing 20 mM 4-chloro-phenylalanine (Sigma-Aldrich), the cells were washed twice with phosphate-buffered saline (PBS) to remove excess media. Resulting colonies were then screened for Erm sensitivity and sequenced to confirm removal of the desired gene and IFDC2 cassette. The process was then repeated for *relQ*, converting the two Δ*relA* Δ*relP* parent strains into *rel*^{0} strains.

Overnight BHI cultures (pre-cultures) were inoculated from single-use aliquots of cryopreserved cells by 1,000-fold dilution. Antibiotics were included in mutant pre-cultures at the aforementioned concentrations or 5 μg mL^{-1} for Tet (Sigma Aldrich). Cultures were then incubated for approximately 18 h at 6% O_2 (Anoxomat jar set to 6% O_2, 7% H_2, 7% CO_2, and 80% N_2) at 37°C. To determine CFUs, samples were sonicated for 90 s using an ultrasonic homogenizer (Biologics, Inc) to disrupt chains prior to dilution in PBS and plated using an Eddy Jet 2 spiral plater (Neutec Group, Inc.). For static growth studies, tubes containing 100% pooled rabbit serum (Gibco) were pre-incubated at 37°C in an atmosphere of 6% O_2. Each tube was then inoculated with a 10^{-6}-fold dilution of the overnight pre-culture, as described above. The inoculated tubes were returned to incubate at the same oxygen concentration. Cultures were removed after 24 h, sonicated, and diluted in PBS prior to plating on BHI agar. Plates were incubated for 24 h in 0% O_2 prior to colony enumeration.

Fermentor Growth Conditions and Sample Collection

A BIOSTAT B bioreactor (Sartorius Stedim) with a 1.5-L capacity UniVessel glass vessel® was used for growth of 800-mL cultures at 37°C, as described in Puccio and Kitten (2020). Briefly, cultures were stirred at 250 rpm and pH was maintained by the automated addition of 2 N KOH (Fisher Chemical). A 40-mL overnight pre-culture of *S. sanguinis* was grown as described above and centrifuged for 10 min at 3,740 × *g* in an Allegra X-142 centrifuge at 4°C (Beckman-Coulter). The supernatant was discarded and the cells were resuspended in BHI prior to inoculation. The air flow was increased stepwise, based on the OD of the fermentor culture. At the peak OD, air flow was increased to 0.50 liters per min, input flow of fresh BHI was set to 17% (∼700 mL h^{-1}) and output flow of waste was set to 34%. Cells were allowed to acclimate to the new conditions for 1 h. The T_{-20} sample was aseptically removed for total RNA isolation or metal analysis (described below). EDTA (Invitrogen) was introduced to the carboy 16 mins later (T_{-4}) to achieve a final concentration of 100 μM. EDTA was then

introduced directly to the vessel 4 min later (T_0), corresponding to the time at which EDTA from the carboy would reach the vessel, to achieve a final concentration of 100 μM. Samples were taken for each post-EDTA time point (T_{10}, T_{25}, T_{50}). In some experiments, $MnSO_4$ or $FeSO_4$ (Puratronic^{TM}; Alfa Aesar) was added to the carboy (T_{66}) and vessel (T_{70}) at a final concentration of 100 μM and samples were taken for metal analysis at T_{80}.

Metal Analysis

Additional 40-mL cell culture samples were collected from WT and Δ*ssaACB* cells at the same fermentor growth time points as described above. The cells were immediately centrifuged at 3,740 × *g* for 10 min at 4°C. The supernatant was decanted and the cell pellet was washed twice with cold cPBS (PBS treated with Chelex-100 resin (Bio-Rad) for 2 h, then filter sterilized and supplemented with EDTA to 1 mM). The pellet was then divided for subsequent acid digestion or protein concentration determination. Trace metal grade (TMG) nitric acid (15%) (Fisher Chemical) was added to one portion of the pellet. The pellet was digested using an Anton Paar microwave digestion system using a modified Organic B protocol: 120°C for 10 min, 180°C for 20 min, with the maximum temperature set to 180°C. The digested samples were then diluted 3-fold with Chelex-treated dH_2O. Metal concentrations were determined using an Agilent 5110 inductively coupled plasma-optical emission spectrometer (ICP-OES). Concentrations were determined by comparison with a standard curve created with a 10 μg mL^{-1} multi-element standard (CMS-5; Inorganic Ventures) diluted in 5% TMG nitric acid. Pb (Inorganic Ventures) was used as an internal standard (10 μg mL^{-1}). The other portion of the pellet was resuspended in PBS and mechanically lysed using a FastPrep-24 instrument with Lysing Matrix B tubes (MP Biomedicals) as described previously (Rhodes et al., 2014). Insoluble material was removed by centrifugation. Protein concentrations were determined using a bicinchoninic acid Protein Assay Kit (Pierce) as recommended by the manufacturer, with bovine serum albumin as the standard. Absorbance was measured in a black, flat-bottom 96-well plate (Greiner) using a microplate reader (BioTek).

Total RNA Isolation

For each RNA sample, 2 mL of fermentor culture was added to 4 mL RNAprotect Bacteria Reagent (Qiagen) and immediately vortexed for 10 s. The sample was then incubated at room temperature for 5–90 min. The samples were then centrifuged for 10 min at 3,740 × *g* at 4°C. The supernatant was discarded and the samples stored at −80°C. RNA isolation and on-column DNase treatment were completed using the RNeasy Mini Kit and RNase-Free DNase Kit, respectively (Qiagen). RNA was eluted in 50 μL RNase-Free water (Qiagen). A second DNase treatment was then performed on the samples (Invitrogen). Total RNA was quantified and purity was assessed using a Nanodrop 2000 Spectrophotometer (Thermo Fisher Scientific).

RNA-Seq Library Preparation and Sequencing

Total RNA quantity and integrity were determined using an Agilent Bioanalyzer RNA Pico assay. All samples passed quality control assessment with RNA Integrity Numbers (RIN) above 8. Two sequential rounds of ribosomal reduction were then performed on all samples using Illumina's Ribo-Zero rRNA Removal Kit. The resulting depleted RNA was assessed using an Agilent Bioanalyzer RNA Pico assay to confirm efficient rRNA removal. Stranded RNA-seq library construction was then performed on the rRNA-depleted RNA using the Ultra II Directional RNA Library Prep Kit for Illumina (New England Biolabs), following manufacturer's specifications for library construction and multiplexing. Final Illumina libraries were assessed for quality using an Agilent Bioanalyzer DNA High Sensitivity Assay and qPCR quantification was performed using NEBNext Library Quant kit for Illumina (New England Biolabs). Individual libraries were pooled equimolarly, and the final pool was sequenced on an Illumina MiSeq, with 2 × 150-bp paired-end reads. Demultiplexing was performed on the Illumina MiSeq's on-board computer and resulting demultiplexed files uploaded to Illumina BaseSpace for data delivery. The University of Virginia Department of Biology Genomics Core Facility (Charlottesville, Virginia) completed all RNA-seq library preparation and sequencing.

RNA-Seq Analysis Pipeline

Using Geneious 11.1 (RRID:SCR_010519)[2], sequence reads were paired and then trimmed using the BBDuk Trimmer prior to mapping to a modified SK36 genome, in which the *ssaACB* operon was replaced with the *aphA-3* sequence. The locus tags are from the Genbank annotation (Benson et al., 2013) available at the time; the annotations were updated shortly before publication and the new locus tags are included in **Supplementary Table S1** for reference. PATRIC annotations (RRID:SCR_004154)[3] (Wattam et al., 2017) are also included for reference. Reads for each post-EDTA sample were compared to the corresponding pre-EDTA (T_{-20}) sample using DESeq2 (Love et al., 2014) (RRID: SCR_015687) in Geneious to determine $\log_2$ fold changes and adjusted *P*-values. Principal component analysis was completed using R (version 3.6.1) and RStudio (version 1.2.5033-1) with Bioconductor (Bioconductor, RRID:SCR_006442) package pcaExplorer version 2.13.0 (Marini and Binder, 2019). Volcano plots were generated using R and RStudio with Bioconductor package EnhancedVolcano (Blighe et al., 2018). All DEGs were input into the DAVID database (RRID:SCR_001881)[4] (Dennis et al., 2003). The KEGG_pathway option was chosen for functional annotation clustering. The *P*-value shows the significance of pathway enrichment. **Figure 2C** was generated using an R script[5].

[2]https://www.geneious.com

[3]https://patricbrc.org/

[4]https://david.ncifcrf.gov/summary.jsp

[5]https://github.com/DrBinZhu/DAVID_FIG

Hydrogen Peroxide Quantification

Culture supernatants without RNAprotect were collected at each time point and stored at −20°C. Hydrogen peroxide concentration was measured using a Fluorometric Hydrogen Peroxide Assay Kit (Sigma). Standards were prepared from 3% hydrogen peroxide provided with the kit as recommended by the manufacturer. Fluorescence was measured in a black-walled, flat-bottom 96-well plate (Greiner) using a microplate reader (BioTek).

Data Analysis and Presentation

All statistical tests, excluding RNA-seq DESeq2 calculations, were performed in GraphPad InStat[6]. Significance was determined by analysis of variance (ANOVA) as indicated in the figure legends. For ANOVA, a Tukey-Kramer test for multiple comparisons was used when $P \leq 0.05$. DESeq2 calculations were completed in Geneious 11.1 or in the pcaExplorer R package, as indicated above. Confidence intervals (95%) of replicate samples were determined by the pcaExplorer R package. $P \leq 0.05$ were considered significant. All graphs and the heat map were constructed using GraphPad Prism[6]; **Figure 7** was made using Biorender.com.

DATA AVAILABILITY STATEMENT

The data discussed in this publication have been deposited in NCBI's Gene Expression Omnibus (Edgar et al., 2002) and are accessible through GEO Series accession number GSE150593 (https://www.ncbi.nlm.nih.gov/geo/query/acc.cgi?acc=GSE150593).

AUTHOR CONTRIBUTIONS

TP and TK designed the experiments and wrote all drafts of the manuscript. TP and KK performed the experiments. TP, KK, and BZ generated the figures. TP, TK, KK, BZ, and PX analyzed the data. All authors reviewed and approved the final version of the manuscript.

[6] graphpad.com

FUNDING

This work was supported by the National Institutes of Health: award no. R01 AI114926 to TK from the National Institute of Allergy and Infectious Diseases; awards no. R01 DE023078 to PX and no. F31 DE028468 to TP from the National Institute of Dental and Craniofacial Research. The content is solely the responsibility of the authors and does not necessarily represent the official views of the National Institutes of Health.

ACKNOWLEDGMENTS

We gratefully acknowledge Shannon Green, Seon-Sook An, Brittany Spivey, and Rachel Korba for meaningful discussions and assistance with experiments. We appreciate Jody Turner (VCU Department of Chemistry) for advice and technical support regarding ICP-OES. We thank Jens Kreth and Nyssa Cullin (Oregon Health & Science University) for providing the IFDC2 *S. sanguinis* strain and corresponding protocol and Stephanie Neal for construction of JFP169.

SUPPLEMENTARY MATERIAL

The Supplementary Material for this article can be found online at: https://www.frontiersin.org/articles/10.3389/fmicb.2020.592615/full#supplementary-material

Supplementary Table 1 | RNA-seq Analysis.

Supplementary Table 2 | Analysis of putative *cre* sites and CcpA regulon.

Supplementary Table 3 | Primers used in this study.

Supplementary Data Sheet 1 | Figures, Methods, and References.

REFERENCES

Ajdic, D., and Pham, V. T. (2007). Global transcriptional analysis of *Streptococcus mutans* sugar transporters using microarrays. *J. Bacteriol.* 189, 5049–5059. doi: 10.1128/JB.00338-07

Bai, Y., Shang, M., Xu, M., Wu, A., Sun, L., and Zheng, L. (2019). Transcriptome, phenotypic, and virulence analysis of *Streptococcus sanguinis* SK36 wild type and its CcpA-null derivative (ΔCcpA). *Front. Cell Infect. Microbiol.* 9:411. doi: 10.3389/fcimb.2019.00411

Baker, S. P., Nulton, T. J., and Kitten, T. (2019). Genomic, phenotypic, and virulence analysis of *Streptococcus sanguinis* oral and infective-endocarditis isolates. *Infect. Immun.* 87:e00703-18. doi: 10.1128/IAI.00703-18

Barnese, K., Gralla, E. B., Cabelli, D. E., and Valentine, J. S. (2008). Manganous phosphate acts as a superoxide dismutase. *JACS* 130, 4604–4606. doi: 10.1021/ja710162n

Barnese, K., Gralla, E. B., Valentine, J. S., and Cabelli, D. E. (2012). Biologically relevant mechanism for catalytic superoxide removal by simple manganese compounds. *Proc. Natl. Acad. Sci. U.S.A.* 109, 6892–6897. doi: 10.1073/pnas.1203051109

Bashore, T. M., Cabell, C., and Fowler, V. Jr. (2006). Update on infective endocarditis. *Curr. Probl. Cardiol.* 31, 274–352. doi: 10.1016/j.cpcardiol.2005.12.001

Bayle, L., Chimalapati, S., Schoehn, G., Brown, J., Vernet, T., and Durmort, C. (2011). Zinc uptake by *Streptococcus pneumoniae* depends on both AdcA and AdcAII and is essential for normal bacterial morphology and virulence. *Mol. Microbiol.* 82, 904–916. doi: 10.1111/j.1365-2958.2011.07862.x

Belda-Ferre, P., Alcaraz, L. D., Cabrera-Rubio, R., Romero, H., Simon-Soro, A., Pignatelli, M., et al. (2012). The oral metagenome in health and disease. *ISME J.* 6, 46–56. doi: 10.1038/ismej.2011.85

Bensing, B. A., Li, L., Yakovenko, O., Wong, M., Barnard, K. N., Iverson, T. M., et al. (2019). Recognition of specific sialoglycan structures by oral streptococci impacts the severity of endocardial infection. *PLoS Pathog.* 15:e1007896. doi: 10.1371/journal.ppat.1007896

Bensing, B. A., Li, Q., Park, D., Lebrilla, C. B., and Sullam, P. M. (2018). Streptococcal Siglec-like adhesins recognize different subsets of human plasma glycoproteins: implications for infective endocarditis. *Glycobiology* 28, 601–611. doi: 10.1093/glycob/cwy052

Benson, D. A., Cavanaugh, M., Clark, K., Karsch-Mizrachi, I., Lipman, D. J., Ostell, J., et al. (2013). GenBank. *Nucleic Acids Res.* 41, D36–D42. doi: 10.1093/nar/gks1195

Bersch, B., Bougault, C., Roux, L., Favier, A., Vernet, T., and Durmort, C. (2013). New insights into histidine triad proteins: solution structure of a *Streptococcus pneumoniae* PhtD domain and zinc transfer to AdcAII. *PLoS One* 8:e81168. doi: 10.1371/journal.pone.0081168

Blighe, K., Rana, S., and Lewis, M. (2018). *EnhancedVolcano: Publication-ready Volcano Plots with Enhanced Colouring and Labeling [Online]*. Available online at: https://github.com/kevinblighe/EnhancedVolcano (accessed on 10 January 2020).

Bor, D. H., Woolhandler, S., Nardin, R., Brusch, J., and Himmelstein, D. U. (2013). Infective endocarditis in the U.S., 1998-2009: a nationwide study. *PLoS One* 8:e60033. doi: 10.1371/journal.pone.0060033

Brenot, A., King, K. Y., and Caparon, M. G. (2005). The PerR regulon in peroxide resistance and virulence of *Streptococcus pyogenes*. *Mol. Microbiol.* 55, 221–234. doi: 10.1111/j.1365-2958.2004.04370.x

Burcham, L. R., Hill, R. A., Caulkins, R. C., Emerson, J. P., Nanduri, B., Rosch, J. W., et al. (2020). *Streptococcus pneumoniae* metal homeostasis alters cellular metabolism. *Metallomics* 12, 1416–1427. doi: 10.1039/d0mt00118j

Burne, R. A., and Chen, Y.-Y. M. (1998). The use of continuous flow bioreactors to explore gene expression and physiology of suspended and adherent populations of oral streptococci. *Methods Cell Sci.* 20, 181–190. doi: 10.1007/978-94-017-2258-2_20

Cahill, T. J., Baddour, L. M., Habib, G., Hoen, B., Salaun, E., Pettersson, G. B., et al. (2017). Challenges in infective endocarditis. *J. Am. Coll. Cardiol.* 69, 325–344. doi: 10.1016/j.jacc.2016.10.066

Chen, L., Ge, X., Dou, Y., Wang, X., Patel, J. R., and Xu, P. (2011). Identification of hydrogen peroxide production-related genes in *Streptococcus sanguinis* and their functional relationship with pyruvate oxidase. *Microbiology* 157, 13–20. doi: 10.1099/mic.0.039669-0

Chen, L., Ge, X., Wang, X., Patel, J. R., and Xu, P. (2012). SpxA1 involved in hydrogen peroxide production, stress tolerance and endocarditis virulence in *Streptococcus sanguinis*. *PLoS One* 7:e40034. doi: 10.1371/journal.pone.0040034

Chen, Y. M., Chiang, Y. C., Tseng, T. Y., Wu, H. Y., Chen, Y. Y., Wu, C. H., et al. (2019). Molecular and functional analysis of the type IV pilus gene cluster in *Streptococcus sanguinis* SK36. *Appl. Environ. Microbiol.* 85:e02788-18. doi: 10.1128/AEM.02788-18

Cheng, X., Redanz, S., Cullin, N., Zhou, X., Xu, X., Joshi, V., et al. (2018). Plasticity of the pyruvate node modulates hydrogen peroxide production and acid tolerance in multiple oral streptococci. *Appl. Environ. Microbiol.* 84:e01697-17. doi: 10.1128/AEM.01697-17

Colomer-Winter, C., Flores-Mireles, A. L., Kundra, S., Hultgren, S. J., and Lemos, J. A. (2019). (p)ppGpp and CodY promote *Enterococcus faecalis* virulence in a murine model of catheter-associated urinary tract infection. *mSphere* 4:e00392-19. doi: 10.1128/mSphere.00392-19

Colomer-Winter, C., Gaca, A. O., and Lemos, J. A. (2017). Association of metal homeostasis and (p)ppGpp regulation in the pathophysiology of *Enterococcus faecalis*. *Infect. Immun.* 85:e00260-17. doi: 10.1128/IAI.00260-17

Cotruvo, J. A. Jr., and Stubbe, J. (2012). Metallation and mismetallation of iron and manganese proteins *in vitro* and *in vivo*: the class I ribonucleotide reductases as a case study. *Metallomics* 4, 1020–1036. doi: 10.1039/c2mt20142a

Crump, K. E., Bainbridge, B., Brusko, S., Turner, L. S., Ge, X., Stone, V., et al. (2014). The relationship of the lipoprotein SsaB, manganese and superoxide dismutase in *Streptococcus sanguinis* virulence for endocarditis. *Mol. Microbiol.* 92, 1243–1259. doi: 10.1111/mmi.12625

Das, S., Kanamoto, T., Ge, X., Xu, P., Unoki, T., Munro, C. L., et al. (2009). Contribution of lipoproteins and lipoprotein processing to endocarditis virulence in *Streptococcus sanguinis*. *J. Bacteriol.* 191, 4166–4179. doi: 10.1128/JB.01739-08

Dayer, M., and Thornhill, M. (2018). Is antibiotic prophylaxis to prevent infective endocarditis worthwhile? *J. Infect. Chemother.* 24, 18–24. doi: 10.1016/j.jiac.2017.10.006

Dennis, G. Jr., Sherman, B. T., Hosack, D. A., Yang, J., Gao, W., et al. (2003). DAVID: Database for Annotation, Visualization, and Integrated Discovery. *Genome Biol.* 4:3.

Dintilhac, A., and Claverys, J.-P. (1997). The *adc* locus, which affects competence for genetic transformation in *Streptococcus pneumoniae*, encodes an ABC transporter with a putative lipoprotein homologous to a family of streptococcal adhesins. *Res. Microbiol.* 148, 119–131. doi: 10.1016/S0923-2508(97)87643-7

Dodds, D. R. (2017). Antibiotic resistance: a current epilogue. *Biochem. Pharmacol.* 134, 139–146. doi: 10.1016/j.bcp.2016.12.005

Edgar, R., Domrachev, M., and Lash, A. E. (2002). Gene expression omnibus: NCBI gene expression and hybridization array data repository. *Nucleic Acids Res.* 30, 207–210. doi: 10.1093/nar/30.1.207

Eijkelkamp, B. A., McDevitt, C. A., and Kitten, T. (2015). Manganese uptake and streptococcal virulence. *Biometals* 28, 491–508. doi: 10.1007/s10534-015-9826-z

Eijkelkamp, B. A., Morey, J. R., Ween, M. P., Ong, C. L., McEwan, A. G., Paton, J. C., et al. (2014). Extracellular zinc competitively inhibits manganese uptake and compromises oxidative stress management in *Streptococcus pneumoniae*. *PLoS One* 9:e89427. doi: 10.1371/journal.pone.0089427

Forner, L., Larsen, T., Kilian, M., and Holmstrup, P. (2006). Incidence of bacteremia after chewing, tooth brushing and scaling in individuals with periodontal inflammation. *J. Clin. Periodontol.* 33, 401–407. doi: 10.1111/j.1600-051X.2006.00924.x

Fox, K. A., Ramesh, A., Stearns, J. E., Bourgogne, A., Reyes-Jara, A., Winkler, W. C., et al. (2009). Multiple posttranscriptional regulatory mechanisms partner to control ethanolamine utilization in *Enterococcus faecalis*. *Proc. Natl. Acad. Sci. U.S.A.* 106, 4435–4440. doi: 10.1073/pnas.0812194106

Garcia-Mendoza, A., Liebana, J., Castillo, A. M., Higuera, A. D. L., and Piedrola, G. (1993). Evaluation of the capacity of oral streptococci to produce hydrogen peroxide. *J. Med. Microbiol.* 39, 434–439. doi: 10.1099/00222615-39-6-434

Giacaman, R. A., Torres, S., Gomez, Y., Munoz-Sandoval, C., and Kreth, J. (2015). Correlation of *Streptococcus mutans* and *Streptococcus sanguinis* colonization and *ex vivo* hydrogen peroxide production in carious lesion-free and high caries adults. *Arch. Oral Biol.* 60, 154–159. doi: 10.1016/j.archoralbio.2014.09.007

Gong, T., Zeng, J., Tang, B., Zhou, X., and Li, Y. (2020). CRISPR-Cas systems in oral microbiome: from immune defense to physiological regulation. *Mol. Oral Microbiol.* 35, 41–48. doi: 10.1111/omi.12279

Gorke, B., and Stulke, J. (2008). Carbon catabolite repression in bacteria: many ways to make the most out of nutrients. *Nat. Rev. Microbiol.* 6, 613–624. doi: 10.1038/nrmicro1932

Gratani, F. L., Horvatek, P., Geiger, T., Borisova, M., Mayer, C., Grin, I., et al. (2018). Regulation of the opposing (p)ppGpp synthetase and hydrolase activities in a bifunctional RelA/SpoT homologue from *Staphylococcus aureus*. *PLoS Genet.* 14:e1007514. doi: 10.1371/journal.pgen.1007514

Griffen, A. L., Beall, C. J., Campbell, J. H., Firestone, N. D., Kumar, P. S., Yang, Z. K., et al. (2012). Distinct and complex bacterial profiles in human periodontitis and health revealed by 16S pyrosequencing. *ISME J.* 6, 1176–1185. doi: 10.1038/ismej.2011.191

Gross, E. L., Beall, C. J., Kutsch, S. R., Firestone, N. D., Leys, E. J., and Griffen, A. L. (2012). Beyond *Streptococcus mutans*: dental caries onset linked to multiple species by 16S rRNA community analysis. *PLoS One* 7:e47722. doi: 10.1371/journal.pone.0047722

Ho, S. N., Hunt, H. D., Horton, R. M., Pullen, J. K., and Pease, L. R. (1989). Site-directed mutagenesis by overlap extension using the polymerase chain reaction. *Gene* 77, 51–59. doi: 10.1016/0378-1119(89)90358-2

Hogg, T., Mechold, U., Malke, H., Cashel, M., and Hilgenfeld, R. (2004). Conformational antagonism between opposing active sites in a bifunctional RelA/SpoT homolog modulates (p)ppGpp metabolism during the stringent response. *Cell* 117, 57–68. doi: 10.1016/s0092-8674(04)00260-0

Irving, S. E., and Corrigan, R. M. (2018). Triggering the stringent response: signals responsible for activating (p)ppGpp synthesis in bacteria. *Microbiology* 164, 268–276. doi: 10.1099/mic.0.000621

Jakubovics, N. S., Smith, A. W., and Jenkinson, H. F. (2002). Oxidative stress tolerance is manganese (Mn^{2+})-regulated in *Streptococcus gordonii*. *Microbiology* 148, 3255–3263. doi: 10.1099/00221287-148-10-3255

Jamil, M., Sultan, I., Gleason, T. G., Navid, F., Fallert, M. A., Suffoletto, M. S., et al. (2019). Infective endocarditis: trends, surgical outcomes, and controversies. *J. Thorac. Dis.* 11, 4875–4885. doi: 10.21037/jtd.2019.10.45

Jeske, L., Placzek, S., Schomburg, I., Chang, A., and Schomburg, D. (2019). BRENDA in 2019: a European ELIXIR core data resource. *Nucleic Acids Res.* 47, D542–D549. doi: 10.1093/nar/gky1048

Kajfasz, J. K., Katrak, C., Ganguly, T., Vargas, J., Wright, L., Peters, Z. T., et al. (2020). Manganese uptake, mediated by SloABC and MntH, is essential for the

fitness of *Streptococcus mutans*. *mSphere* 5:e00764-19. doi: 10.1128/mSphere.00764-19

Kallio, A., Sepponen, K., Hermand, P., Denoel, P., Godfroid, F., and Melin, M. (2014). Role of pneumococcal histidine triad (Pht) proteins in attachment of *Streptococcus pneumoniae* to respiratory epithelial cells. *Infect. Immun.* 82, 1683–1691. doi: 10.1128/IAI.00699-13

Kanehisa, M., and Goto, S. (2000). KEGG: Kyoto Encyclopedia of Genes and Genomes. *Nucleic Acids Res.* 28, 27–30. doi: 10.1093/nar/28.1.27

Kaspar, J., Kim, J. N., Ahn, S. J., and Burne, R. A. (2016). An essential role for (p)ppGpp in the integration of stress tolerance, peptide signaling, and competence development in *Streptococcus mutans*. *Front. Microbiol.* 7:1162. doi: 10.3389/fmicb.2016.01162

Kaval, K. G., and Garsin, D. A. (2018). Ethanolamine utilization in bacteria. *mBio* 9:e00066-18. doi: 10.1128/mBio.00066-18

Kaval, K. G., Gebbie, M., Goodson, J. R., Cruz, M. R., Winkler, W. C., and Garsina, D. A. (2019). Ethanolamine utilization and bacterial microcompartment formation are subject to carbon catabolite repression. *J. Bacteriol.* 201:e00703-18. doi: 10.1128/JB

Kazmierczak, K. M., Wayne, K. J., Rechtsteiner, A., and Winkler, M. E. (2009). Roles of *relSpn* in stringent response, global regulation and virulence of serotype 2 *Streptococcus pneumoniae* D39. *Mol. Microbiol.* 72, 590–611. doi: 10.1111/j.1365-2958.2009.06669.x

Kehres, D. G., and Maguire, M. E. (2003). Emerging themes in manganese transport, biochemistry and pathogenesis in bacteria. *FEMS Microbiol. Rev.* 27, 263–290. doi: 10.1016/s0168-6445(03)00052-4

Kholy, K. E., Genco, R. J., and Van Dyke, T. E. (2015). Oral infections and cardiovascular disease. *Trends Endocrinol. Metab.* 26, 315–321. doi: 10.1016/j.tem.2015.03.001

Kim, J. N., Ahn, S. J., Seaton, K., Garrett, S., and Burne, R. A. (2012). Transcriptional organization and physiological contributions of the *relQ* operon of *Streptococcus mutans*. *J. Bacteriol.* 194, 1968–1978. doi: 10.1128/jb.00037-12

Kinane, D. F., Riggio, M. P., Walker, K. F., MacKenzie, D., and Shearer, B. (2005). Bacteraemia following periodontal procedures. *J. Clin. Periodontol.* 32, 708–713. doi: 10.1111/j.1600-051X.2005.00741.x

Kolenbrander, P. E., Palmer, R. J. Jr., Periasamy, S., and Jakubovics, N. S. (2010). Oral multispecies biofilm development and the key role of cell-cell distance. *Nat. Rev. Microbiol.* 8, 471–480. doi: 10.1038/nrmicro2381

Kreth, J., Merritt, J., Shi, W., and Qi, F. (2005). Competition and coexistence between *Streptococcus mutans* and *Streptococcus sanguinis* in the dental biofilm. *J. Bacteriol.* 187, 7193–7203. doi: 10.1128/JB.187.21.7193-7203.2005

Kreth, J., Zhang, Y., and Herzberg, M. C. (2008). Streptococcal antagonism in oral biofilms: *Streptococcus sanguinis* and *Streptococcus gordonii* interference with *Streptococcus mutans*. *J. Bacteriol.* 190, 4632–4640. doi: 10.1128/jb.00276-08

Kuipers, K., Gallay, C., Martinek, V., Rohde, M., Martinkova, M., van der Beek, S. L., et al. (2016). Highly conserved nucleotide phosphatase essential for membrane lipid homeostasis in *Streptococcus pneumoniae*. *Mol. Microbiol.* 101, 12–26. doi: 10.1111/mmi.13312

Lee, S., Kim, K.-K., and Choe, S.-J. (2001). Binding of oral streptococci to human fibrinogen. *Oral Microbiol. Immunol.* 16, 88–93. doi: 10.1034/j.1399-302x.2001.016002088.x

Lemos, J. A., Lin, V. K., Nascimento, M. M., Abranches, J., and Burne, R. A. (2007). Three gene products govern (p)ppGpp production by *Streptococcus mutans*. *Mol. Microbiol.* 65, 1568–1581. doi: 10.1111/j.1365-2958.2007.05897.x

Liochev, S. I., and Fridovich, I. (2004). Carbon dioxide mediates Mn(II)-catalyzed decomposition of hydrogen peroxide and peroxidation reactions. *Proc. Natl. Acad. Sci. U.S.A.* 101, 12485–12490. doi: 10.1073/pnas.0404911101

Lockhart, P. B., Brennan, M. T., Sasser, H. C., Fox, P. C., Paster, B. J., and Bahrani-Mougeot, F. K. (2008). Bacteremia associated with toothbrushing and dental extraction. *Circulation* 117, 3118–3125. doi: 10.1161/CIRCULATIONAHA.107.758524

Love, M. I., Huber, W., and Anders, S. (2014). Moderated estimation of fold change and dispersion for RNA-seq data with DESeq2. *Genome Biol.* 15:550. doi: 10.1186/s13059-014-0550-8

Makarova, K. S., Wolf, Y. I., Alkhnbashi, O. S., Costa, F., Shah, S. A., Saunders, S. J., et al. (2015). An updated evolutionary classification of CRISPR-Cas systems. *Nat. Rev. Microbiol.* 13, 722–736. doi: 10.1038/nrmicro3569

Makhlynets, O., Boal, A. K., Rhodes, D. V., Kitten, T., Rosenzweig, A. C., and Stubbe, J. (2014). *Streptococcus sanguinis* class Ib ribonucleotide reductase: high activity with both iron and manganese cofactors and structural insights. *J. Biol. Chem.* 289, 6259–6272. doi: 10.1074/jbc.M113.533554

Marini, F., and Binder, H. (2019). pcaExplorer: an R/Bioconductor package for interacting with RNA-seq principal components. *BMC Bioinform.* 20:331. doi: 10.1186/s12859-019-2879-1

Martin, J. E., and Giedroc, D. P. (2016). Functional determinants of metal ion transport and selectivity in paralogous cation diffusion facilitator transporters CzcD and MntE in *Streptococcus pneumoniae*. *J. Bacteriol.* 198, 1066–1076. doi: 10.1128/JB.00975-15

Martin, J. E., Le, M. T., Bhattarai, N., Capdevila, D. A., Shen, J., Winkler, M. E., et al. (2019). A Mn-sensing riboswitch activates expression of a Mn^{2+}/Ca^{2+} ATPase transporter in *Streptococcus*. *Nucleic Acids Res.* 47, 6885–6899. doi: 10.1093/nar/gkz494

Martin, J. E., Lisher, J. P., Winkler, M. E., and Giedroc, D. P. (2017). Perturbation of manganese metabolism disrupts cell division in *Streptococcus pneumoniae*. *Mol. Microbiol.* 104, 334–348. doi: 10.1111/mmi.13630

Mechold, U., Gentry, D., Cashel, M., Steiner, K., and Malke, H. (1996). Functional analysis of a *relA/spoT* gene homolog from *Streptococcus equisimilis*. *J. Bacteriol.* 178, 1401–1411. doi: 10.1128/jb.178.5.1401-1411.1996

Moraes, J. J., Stipp, R. N., Harth-Chu, E. N., Camargo, T. M., Hofling, J. F., and Mattos-Graner, R. O. (2014). Two-component system VicRK regulates functions associated with establishment of *Streptococcus sanguinis* in biofilms. *Infect. Immun.* 82, 4941–4951. doi: 10.1128/IAI.01850-14

Moreillon, P., and Que, Y.-A. (2004). Infective endocarditis. *Lancet* 363, 139–149. doi: 10.1016/s0140-6736(03)15266-x

Moreillon, P., Que, Y. A., and Bayer, A. S. (2002). Pathogenesis of streptococcal and staphylococcal endocarditis. *Infect. Dis. Clin. North Am.* 16, 297–318. doi: 10.1016/s0891-5520(01)00009-5

Murgas, C. J., Green, S. P., Forney, A. K., Korba, R. M., An, S. S., Kitten, T., et al. (2020). Intracellular metal speciation in *Streptococcus sanguinis* establishes SsaACB as critical for redox maintenance. *ACS Infect. Dis.* 6, 1906–1921. doi: 10.1021/acsinfecdis.0c00132

Nascimento, M. M., Lemos, J. A., Abranches, J., Lin, V. K., and Burne, R. A. (2008). Role of RelA of *Streptococcus mutans* in global control of gene expression. *J. Bacteriol.* 190, 28–36. doi: 10.1128/JB.01395-07

Nies, D. H. (1992). CzcR and CzcD, gene products affecting regulation of resistance to cobalt, zinc, and cadmium (*czc* system) in *Alcaligenes eutrophus*. *J. Bacteriol.* 174, 8102–8110. doi: 10.1128/jb.174.24.8102-8110.1992

Novichkov, P. S., Kazakov, A. E., Ravcheev, D. A., Leyn, S. A., Kovaleva, G. Y., Sutormin, R. A., et al. (2013). RegPrecise 3.0 - A resource for genome-scale exploration of transcriptional regulation in bacteria. *BMC Genomics* 14:745. doi: 10.1186/1471-2164-14-745

Ogunniyi, A. D., Mahdi, L. K., Jennings, M. P., McEwan, A. G., McDevitt, C. A., Van der Hoek, M. B., et al. (2010). Central role of manganese in regulation of stress responses, physiology, and metabolism in *Streptococcus pneumoniae*. *J. Bacteriol.* 192, 4489–4497. doi: 10.1128/JB.00064-10

Paik, S., Senty, L., Das, S., Noe, J. C., Munro, C. L., and Kitten, T. (2005). Identification of virulence determinants for endocarditis in *Streptococcus sanguinis* by signature-tagged mutagenesis. *Infect. Immun.* 73, 6064–6074. doi: 10.1128/IAI.73.9.6064-6074.2005

Papp-Wallace, K. M., and Maguire, M. E. (2006). Manganese transport and the role of manganese in virulence. *Annu. Rev. Microbiol.* 60, 187–209. doi: 10.1146/annurev.micro.60.080805.142149

Parker, M. W., and Blake, C. C. F. (1988). Iron- and manganese-containing superoxide dismutases can be distinguished by analysis of their primary structures. *FEBS Lett.* 229, 377–382. doi: 10.1016/0014-5793(88)81160-8

Perrin, D. D., and Dempsey, B. (1974). *Buffers for pH and Metal Ion Control*. Bristol: J. W. Arrowsmith Ltd.

Plumptre, C. D., Eijkelkamp, B. A., Morey, J. R., Behr, F., Counago, R. M., Ogunniyi, A. D., et al. (2014). AdcA and AdcAII employ distinct zinc acquisition mechanisms and contribute additively to zinc homeostasis in *Streptococcus pneumoniae*. *Mol. Microbiol.* 91, 834–851. doi: 10.1111/mmi.12504

Poyart, C., Quesne, G., Coulon, S., Berche, P., and Trieu-Cuot, P. (1988). Identification of streptococci to species level by sequencing the gene encoding

the manganese-dependent superoxide dismutase. *J. Clin. Microbiol.* 36, 41–47. doi: 10.1128/jcm.36.1.41-47.1998

Puccio, T., and Kitten, T. (2020). Fermentor growth of *Streptococcus sanguinis*. *Protocols.io.* doi: 10.17504/protocols.io.bkayksfw

Puccio, T., Misra, B. B., and Kitten, T. (2020). Time-course analysis of *Streptococcus sanguinis* after manganese depletion reveals changes in glycolytic, nucleotide, and redox metabolites. *bioRxiv* doi: 10.1101/2020.08.30.274233

Pulliainen, A. T., Haataja, S., Kahkonen, S., and Finne, J. (2003). Molecular basis of H_2O_2 resistance mediated by streptococcal Dpr: demonstration of the functional involvement of the putative ferroxidase center by site-directed mutagenesis in *Streptococcus suis*. *J. Biol. Chem.* 278, 7996–8005. doi: 10.1074/jbc.M210174200

Quan, T. P., Muller-Pebody, B., Fawcett, N., Young, B. C., Minaji, M., Sandoe, J., et al. (2020). Investigation of the impact of the NICE guidelines regarding antibiotic prophylaxis during invasive dental procedures on the incidence of infective endocarditis in England: an electronic health records study. *BMC Med.* 18:84. doi: 10.1186/s12916-020-01531-y

Radin, J. N., J. L. Kelliher, P. K. Parraga Solorzano, and T. E. Kehl-Fie. (2016). The two-component system ArlRS and alterations in metabolism enable *Staphylococcus aureus* to resist calprotectin-induced manganese starvation. PLoS Pathog 12:e1006040. doi: 10.1371/journal.ppat.1006040

Redanz, S., Masilamani, R., Cullin, N., Giacaman, R. A., Merritt, J., and Kreth, J. (2018). Distinct regulatory role of carbon catabolite protein A (CcpA) in oral streptococcal *spxB* expression. *J. Bacteriol.* 200:e00619-17. doi: 10.1128/JB.00619-17

Rhodes, D. V., Crump, K. E., Makhlynets, O., Snyder, M., Ge, X., Xu, P., et al. (2014). Genetic characterization and role in virulence of the ribonucleotide reductases of *Streptococcus sanguinis*. *J. Biol. Chem.* 289, 6273–6287. doi: 10.1074/jbc.M113.533620

Rosch, J. W., Gao, G., Ridout, G., Wang, Y. D., and Tuomanen, E. I. (2009). Role of the manganese efflux system *mntE* for signalling and pathogenesis in *Streptococcus pneumoniae*. *Mol. Microbiol.* 72, 12–25. doi: 10.1111/j.1365-2958.2009.06638.x

Seaton, K., Ahn, S. J., Sagstetter, A. M., and Burne, R. A. (2011). A transcriptional regulator and ABC transporters link stress tolerance, (p)ppGpp, and genetic competence in *Streptococcus mutans*. *J. Bacteriol.* 193, 862–874. doi: 10.1128/JB.01257-10

Shields, R. C., Walker, A. R., Maricic, N., Chakraborty, B., Underhill, S. A. M., and Burne, R. A. (2020). Repurposing the *Streptococcus mutans* CRISPR-Cas9 system to understand essential gene function. *PLoS Pathog.* 16:e1008344. doi: 10.1371/journal.ppat.1008344

Silver, J. G., Martin, A. W., and McBride, B. C. (1977). Experimental transient bacteraemias in human subjects with varying degrees of plaque accumulation and gingival inflammation. *J. Clin. Periodontol.* 4, 92–99. doi: 10.1111/j.1600-051x.1977.tb01888.x

Silver, J. G., Martin, A. W., and McBride, B. C. (1979). Experimental transient bacteraemias in human subjects with clinically healthy gingivae. *J. Clin. Periodontol.* 6, 33–36. doi: 10.1111/j.1600-051x.1979.tb02288.x

Socransky, S. S., Manganiello, A. D., Propas, D., Oram, V., and Houte, J. V. (1977). Bacteriological studies of developing supragingival dental plaque. *J. Periodontal Res.* 12, 90–106. doi: 10.1111/j.1600-0765.1977.tb00112.x

Spellerberg, B., Cundell, D. R., Sandros, J., Pearce, B. J., Idanpaan-Heikkila, I., Rosenow, C., et al. (1996). Pyruvate oxidase, as a determinant of virulence in *Streptococcus pneumoniae*. *Mol. Microbiol.* 19, 803–813. doi: 10.1046/j.1365-2958.1996.425954.x

Sreenivasan, P. K., Tischio-Bereski, D., and Fine, D. H. (2017). Reduction in bacteremia after brushing with a triclosan/copolymer dentifrice-A randomized clinical study. *J. Clin. Periodontol.* 44, 1020–1028. doi: 10.1111/jcpe.12798

Stingu, C. S., Eschrich, K., Rodloff, A. C., Schaumann, R., and Jentsch, H. (2008). Periodontitis is associated with a loss of colonization by *Streptococcus sanguinis*. *J. Med. Microbiol.* 57(Pt 4), 495–499. doi: 10.1099/jmm.0.47649-0

Thornhill, M. H., Gibson, T. B., Cutler, E., Dayer, M. J., Chu, V. H., Lockhart, P. B., et al. (2018). Antibiotic prophylaxis and incidence of endocarditis before and after the 2007 AHA recommendations. *J. Am. Coll. Cardiol.* 72, 2443–2454. doi: 10.1016/j.jacc.2018.08.2178

Turner, L. S., Kanamoto, T., Unoki, T., Munro, C. L., Wu, H., and Kitten, T. (2009). Comprehensive evaluation of *Streptococcus sanguinis* cell wall-anchored proteins in early infective endocarditis. *Infect. Immun.* 77, 4966–4975. doi: 10.1128/IAI.00760-09

Warner, J. B., and Lolkema, J. S. (2003). CcpA-dependent carbon catabolite repression in bacteria. *Microbiol. Mol. Biol. Rev.* 67, 475–490. doi: 10.1128/mmbr.67.4.475-490.2003

Waters, L. S. (2020). Bacterial manganese sensing and homeostasis. *Curr. Opin. Chem. Biol* 55, 96–102. doi: 10.1016/j.cbpa.2020.01.003

Wattam, A. R., Davis, J. J., Assaf, R., Boisvert, S., Brettin, T., Bun, C., et al. (2017). Improvements to PATRIC, the all-bacterial bioinformatics database and analysis resource center. *Nucleic Acids Res.* 45, D535–D542. doi: 10.1093/nar/gkw1017

Widmer, E., Que, Y.-A., Entenza, J. M., and Moreillon, P. (2006). New concepts in the pathophysiology of infective endocarditis. *Curr. Infect. Dis. Rep.* 8, 271–279. doi: 10.1007/s11908-006-0071-z

Wilson, W., Taubert, K. A., Gewitz, M., Lockhart, P. B., Baddour, L. M., Levison, M., et al. (2007). Prevention of infective endocarditis: guidelines from the american heart association. *Circulation* 116, 1736–1754. doi: 10.1161/CIRCULATIONAHA.106.183095

Xie, Z., Okinaga, T., Qi, F., Zhang, Z., and Merritt, J. (2011). Cloning-independent and counterselectable markerless mutagenesis system in *Streptococcus mutans*. *Appl. Environ. Microbiol.* 77, 8025–8033. doi: 10.1128/AEM.06362-11

Xu, P., Alves, J. M., Kitten, T., Brown, A., Chen, Z., Ozaki, L. S., et al. (2007). Genome of the opportunistic pathogen *Streptococcus sanguinis*. *J. Bacteriol.* 189, 3166–3175. doi: 10.1128/JB.01808-06

Xu, P., Ge, X., Chen, L., Wang, X., Dou, Y., Xu, J. Z., et al. (2011). Genome-wide essential gene identification in *Streptococcus sanguinis*. *Sci. Rep.* 1:125. doi: 10.1038/srep00125

Xu, Y., Itzek, A., and Kreth, J. (2014). Comparison of genes required for H_2O_2 resistance in *Streptococcus gordonii* and *Streptococcus sanguinis*. *Microbiology* 160, 2627–2638. doi: 10.1099/mic.0.082156-0

Yamamoto, Y., Higuchi, M., Poole, L. B., and Kamio, Y. (2000). Role of the *dpr* product in oxygen tolerance in *Streptococcus mutans*. *J. Bacteriol.* 182, 3740–3747. doi: 10.1128/jb.182.13.3740-3747.2000

Yamamoto, Y., Poole, L. B., Hantgan, R. R., and Kamio, Y. (2002). An iron-binding protein, Dpr, from *Streptococcus mutans* prevents iron-dependent hydroxyl radical formation *in vitro*. *J. Bacteriol.* 184, 2931–2939. doi: 10.1128/jb.184.11.2931-2939.2002

Yang, N., Xie, S., Tang, N. Y., Choi, M. Y., Wang, Y., and Watt, R. M. (2019). The Ps and Qs of alarmone synthesis in *Staphylococcus aureus*. *PLoS One* 14:e0213630. doi: 10.1371/journal.pone.0213630

Zeng, L., Chen, L., and Burne, R. A. (2018). Preferred hexoses influence long-term memory in and induction of lactose catabolism by *Streptococcus mutans*. *Appl. Environ. Microbiol.* 84:e00864-18. doi: 10.1128/AEM.00864-18

Zheng, L., Chen, Z., Itzek, A., Ashby, M., and Kreth, J. (2011). Catabolite control protein A controls hydrogen peroxide production and cell death in *Streptococcus sanguinis*. *J. Bacteriol.* 193, 516–526. doi: 10.1128/JB.01131-10

Conflict of Interest: The authors declare that the research was conducted in the absence of any commercial or financial relationships that could be construed as a potential conflict of interest.